Chem Soc Rev

REVIEW ARTICLE

View Article Online
View Journal | View Issue

Cite this: *Chem. Soc. Rev.*, 2015, **44**, 7177

The ADOR mechanism for the synthesis of new zeolites

Pavla Eliášová,[a] Maksym Opanasenko,[a] Paul S. Wheatley,[b] Mariya Shamzhy,[a] Michal Mazur,[a] Petr Nachtigall,[c] Wieslaw J. Roth,[ad] Russell E. Morris*[b] and Jiří Čejka*[a]

Received 19th January 2015

DOI: 10.1039/c5cs00045a

www.rsc.org/csr

A novel methodology, called ADOR (assembly–disassembly–organisation–reassembly), for the synthesis of zeolites is reviewed here in detail. The ADOR mechanism stems from the fact that certain chemical weakness against a stimulus may be present in a zeolite framework, which can then be utilized for the preparation of new solids through successive manipulation of the material. In this review, we discuss the critical factors of germanosilicate zeolites required for application of the ADOR protocol and describe the mechanism of hydrolysis, organisation and condensation to form new zeolites starting from zeolite **UTL**. Last but not least, we discuss the potential of this methodology to form other zeolites and the prospects for future investigations.

1. Introduction

Zeolites are inorganic crystalline solids with a microporous framework structure[1,2] suitable for a wide range of host–guest chemistry applications[3,4] such as adsorption and separation,[5–9] ion exchange,[3,4] catalysis,[10–14] and sensor fabrication.[15–17] Originally, zeolites were defined by the mineralogical community as a special class of aluminosilicates with a particular set of properties.[18] Zeolites are currently defined as three-dimensional (3D) materials that possess a regular micropore system and consist of TO_4 tetrahedra (where T besides Si and Al, can be Ge, Ti, B, Ga, P, *etc.*) each having 4 neighbours (4-connected).[19] Structures that are

[a] *J. Heyrovský Institute of Physical Chemistry, Academy of Sciences of Czech Republic, v.v.i. Dolejškova 3, 182 23 Prague 8, Czech Republic. E-mail: jiri.cejka@jh-inst.cas.cz*
[b] *EaStChem School of Chemistry, University of St Andrews, Purdie Building, St Andrews KY16 9ST, UK. E-mail: rem1@st-andrews.ac.uk*
[c] *Department of Physical and Macromolecular Chemistry, Faculty of Science, Charles University in Prague, Hlavova 2030, 12840 Prague 2, Czech Republic*
[d] *Faculty of Chemistry, Jagiellonian University in Kraków, ul. Ingardena 3, 30-060 Kraków, Poland*

Pavla Eliášová

Pavla Eliášová (born Chlubná) obtained her master's degree in Chemistry and Geology at Palackého University in Olomouc in 2010. She continued her PhD study at Charles University in Prague while working at the J. Heyrovský Institute of Physical Chemistry under the supervision of Prof. Jiří Čejka. She received her PhD in 2014. At present she is a Research Fellow in the Center for Nanomaterials and Chemical Reactions at the Institute of Basic Science in Daejeon (Republic of Korea) working in the group of Prof. Ryong Ryoo. Her research interests are zeolites with two-dimensional structures and/or hierarchical porosity for heterogeneous catalysis.

Maksym Opanasenko

Maksym Opanasenko obtained his Mgr degree from the Lomonosov Moscow State University in 2006. He performed his PhD study at the L. V. Pisazhevsky Institute of Physical Chemistry of the National Academy of Sciences of Ukraine, where he defended his PhD Thesis entitled "Structure and sorption properties of porous polymeric and composite materials obtained by matrix polymerization" in 2010. Currently, Dr Opanasenko holds a postdoctoral position at the J. Heyrovsky Institute of Physical Chemistry in the group of Prof. J. Čejka. His current interests are the synthesis of new zeolites and application of porous solids in catalysis.

not fully 4-connected (called interrupted structures) are also considered as members of the broad zeolite family.

Synthetic zeolites are produced almost exclusively under solvothermal conditions, often in the presence of structure-directing agents (SDAs) and mineralizing agents (*e.g.* OH^- and/or F^-).[20,21] Historically, most zeolite syntheses yielded three-dimensional (3D) materials that crystallized directly from the reaction gel.[22] One of the main disadvantages of the prevailing solvothermal approach to the preparation of new zeolites is the limited control over the synthesis process and, as a result, the final structure of the product. This is a consequence of our incomplete understanding of zeolite formation processes, resulting in a methodology that relies heavily on trial and error. To alleviate the lack of predictability, many studies have been performed to provide fundamental knowledge on the influence of parameters such as SDA nature (charge, polarizability, size, branching degree, rigidity), the type of mineralizing agents (OH^-, F^-), and the T/H_2O ratio on the structure of zeolites formed[23–27] or the influence of SDAs on the distribution of acid sites in the framework.[28–30] Much attention has been focused on the understanding of the relationship between frameworks and the molecular structure of the SDA. However, the fact that most SDAs are not as specific as expected proving that other factors (*i.e.* kinetics, chemistry of intermediate species, *etc.*) also influence the nature of the zeolite product formed. The absence of a general recipe for the synthesis of zeolites with predicted structure stimulated ideas about alternative new approaches to control the fabrication of microporous materials.

One of the oldest concepts for the formation 3D frameworks is based on structurally uniform building blocks, SBUs, participating in the assembly.[20] This potentially exploitable mechanism is attractive, but unfortunately has not been very fruitful in practice. The basic issue with this approach is that it simply shifts the problem of making a zeolite to one of making the building units, and then ensuring that the building units connect together to form a zeolite without any rearrangement into other units – this is not always possible to control and even less easy to prove! However, the most promising approach of this kind, which has been developed over the last few years, utilizes layers with zeolite-like structure as the building units. These can then be assembled into a 3D zeolite, under the right conditions, without affecting the layered structure of the building unit. There are several different ways to accomplish this but perhaps the most interesting and, most importantly, the predictable method is the ADOR process (assembly–disassembly–organisation–reassembly) whereby a previously assembled zeolite is selectively and controllably disassembled into layered building units, which are then organised into a suitable orientation before being reassembled into a new zeolite structure (Scheme 1).

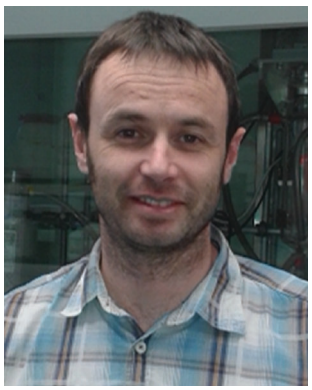

Paul S. Wheatley

Dr Paul Wheatley was born in Kirkcaldy, Scotland, in 1977. He received his BSc and PhD degrees in chemistry from the University of St Andrews in 1999 and 2003, respectively. He is now a senior PDRA and commercialisation liaison in the School of Chemistry at the University of St Andrews. His research interests include the synthesis, characterisation and applications of both zeolites and metal organic frameworks. Research highlights include novel synthetic routes and medical applications of porous solids.

Mariya Shamzhy

Mariya Shamzhy received her Mgr degree in Chemistry from the Lomonosov Moscow State University in 2006. After that, she joined the L. V. Pisazhevsky Institute of Physical Chemistry of the National Academy of Sciences of Ukraine where she received her PhD in 2012, working on the synthesis of extra-large pore germanosilicate zeolites with tunable acidity for catalytic applications. Currently Dr Shamzhy works as an Associate researcher at the J. Heyrovsky Institute of Physical Chemistry of the Academy of Sciences of the Czech Republic. Her main research interests include the synthesis of novel nano-structured materials, heterogeneous catalysis on zeolites, micro-mesoporous materials and metal–organic-frameworks.

Michal Mazur

Michal Mazur received his MSc degree from the Jagiellonian University in Cracow (Poland) at the Faculty of Chemistry in 2012. He is currently completing his PhD in Physical Chemistry at the Charles University in Prague (Czech Republic), working in the J. Heyrovský Institute of Physical Chemistry in Prague at the Department of Synthesis and Catalysis under the supervision of Prof. Jiří Čejka. His research interests involve the synthesis and characterization of layered zeolites and their modifications, especially chemistry of the interlayer space of two-dimensional zeolites.

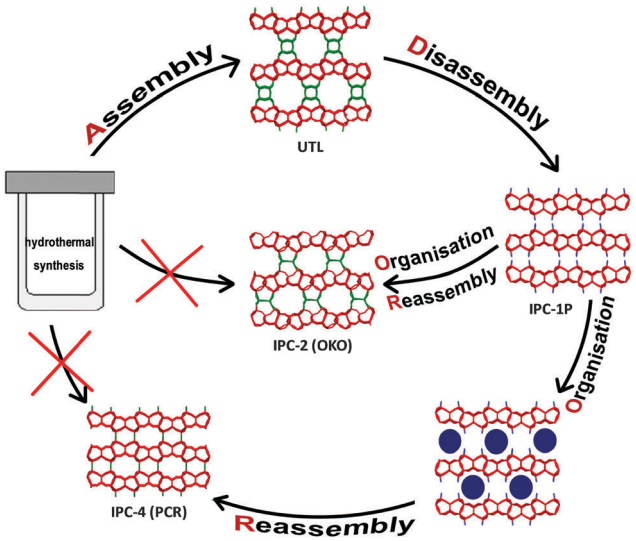

Scheme 1 The ADOR method in a cycle scheme demonstrating the mechanism for the synthesis of two novel zeolites, IPC-2 (**OKO**) and IPC-4 (**PCR**), in which both of them have not been so far prepared by direct hydrothermal synthesis. The inter-layer bonds are highlighted in green, and the terminal silanol groups in blue.

The aim of this review is to describe in detail the ADOR mechanism and to highlight the advantages of this approach from the experimental and theoretical points of view, the key features and requirements for successful manipulation of the layers, and main challenges for the application of the ADOR method in the preparation of new materials.

2. 2D zeolites

Over the last two decades some zeolite syntheses were found to produce two-dimensional (2D) precursors[31–33] having the same basic structure as a 3D framework with separated layers approximately one unit cell thick, typically 1–2 nm, along one direction.[34–38] Generally, the precursors condense topotactically to produce the conventional 3D structures[39] but other monolayer forms have also been discovered such as the **MWW** representatives MCM-56[40] and EMM-10,[41] **MFI** as layered disordered or ordered assemblies,[42,43] self-supported layers[44] and as self-pillared materials.[45] If one considers the possibility of obtaining 3D zeolites by topotactic condensation of 2D "building blocks" a whole new class of zeolites may be prepared simply by the synthesis of novel 2D zeolites and their subsequent condensation. The zeolite framework types **AFO**,[46] **AST**,[47] **MTF**,[48] **MWW**,[49] **RRO**,[50] **RWR**,[51] and **SOD**[52] as well as structurally related pairs having the same layers, differently arranged, **CAS**[53] and **NSI**,[54] **CDO**[55] and **FER**[56] have been obtained from directly synthesized 2D precursors. However, most frameworks known to have a layered precursor can be also synthesized by a direct route. Does this mean that after the successful discovery of a new zeolite *via* the indirect precursor pathway one might expect to find the direct one sooner or later?

The chemistry of layered solids with zeolite-like structures, called 2D zeolites, is very rich as they have been used for the preparation of other new materials *via* intercalation, stabilization, pillaring, and delamination processes.[34,35,37,57,58] At present, between 15 and 20 different structural types constructed from zeolite layers have been identified.[59] However, many are not strictly zeolites by containing additional non 4-connected components.[35] This is a consequence of the geometry of directly synthesized layers, which while they can often be directly condensed into 3D solids they cannot always be guaranteed to do so to yield fully 4-connected materials or like in the case of interlamellar-expanded-zeolite (IEZ) derivatives, containing a SiO_4 link connecting two layers.

At present, there are three main methods to prepare 2D zeolites, (i) traditional direct synthesis, akin to the known methodology for discovering regular zeolite structures, such as the first recognized layered zeolite, MCM-22P,[31,32,60] (ii) synthesis of 2D zeolites using specially designed templates,[42,61] and (iii) a top-down approach starting with an appropriate framework that is conducive to selective degradation into separated layers as demonstrated for zeolite **UTL** – the ADOR method.[62,63]

(i) The direct solvothermal preparation of layered zeolite forms was the first to be discovered and now more than 10 frameworks have been recognized by that route. They may be characterized as analogous to traditional zeolite syntheses but for reasons not fully recognized produce layered species. It may be that framework propagation is being suppressed in the direction perpendicular to the precursor layer, which is possibly due to the low content of aluminium in addition to other favourable circumstances.[57] Zeolite framework **MWW** was the first and most diverse system in providing various layered (2D) forms.[49]

(ii) A remarkable new method of designing 2D zeolites has been recently demonstrated by Ryoo and coworkers.[61,64] The general idea is to use a multifunctional surfactant-SDA comprising charged ammonium groups capable of templating zeolite **MFI**, and a long hydrocarbon chain preventing the growth of adjacent layers. The products obtained this way by the direct synthesis were ultrathin zeolitic nanosheets in multilayered stacks[42,61] as well as self-supported layers.[44] It may be a general approach to the synthesis of layered zeolite forms and indeed other frameworks were attempted this way.[65] However, the evidence that they could produce structures comparable with the spectacular images similar to those of the **MFI** nanosheets is yet to come. This approach is promising to open a way to fabricate materials that allow avoiding the accessibility limitations of existing zeolite catalysts for transformations of bulky molecules.[42,65–68] On the other hand, the layered zeolites obtained by this method are designed to contain SDAs occluded in the micropores, which complicates the separation of the template-covered layers and may limit the possibility for their further utilization as precursors for other 2D zeolite structures.

(iii) The most recent method for the synthesis of 2D zeolites[62,63,69] is the hydrolysis of the pre-formed zeolite as the prerequisite for the ADOR process, a top-down strategy of

controllable disassembly of an appropriate 3D framework to produce a layered precursor. The method exploits the chemical weakness in a framework to separate its constituent layers. It depends on having a suitable structure and composition although one should not preclude *a priori* the possibility of 'unzipping' any zeolite structure in the future. One of the main differences of this approach in comparison with the method using a multifunctional SDA is the absence of the template side chains preventing the manipulation of the layers. The zeolitic precursor obtained in this way can, in principle, be condensed topotactically into a 3D material or transformed into expanded derivatives *via* stabilization/silylation or swelling/pillaring treatments similar to those obtained by route (i).

The ADOR procedure has 4 steps: it starts with the preparation of initial zeolite (assembly), its selective degradation into 2D building-blocks/layers (disassembly), pre-ordering of the layers into suitable orientations (organisation), and finally condensation to a new structure (reassembly). This strategy for the synthesis of new microporous materials was first applied for the preparation of **PCR**- and **OKO**-type zeolites from **UTL** as the parent framework.[63] In the following discussion we will explain the various steps in the ADOR process, concentrating first on its application to **UTL**.

3. The assembly step – zeolite UTL and similar frameworks

Germanosilicate zeolite **UTL** was reported in 2004 as the first extra-large pore zeolite with intersecting 14- and 12-ring channels with pore diameters of 9.5 × 7.1 Å and 8.5 × 5.5 Å, respectively.[70] It was discovered independently at the same time by the research groups of Corma (designated ITQ-15[71]) and Patarin (designated IM-12[72]). ITQ-15 was prepared using 1,1,3-trimethyl-6-azonia-tricyclo-[3.2.1.4^{6,6}]decane hydroxide as the organic SDA while (6*R*,10*S*)-6,10-dimethyl-5-azoniaspiro[4.5]decane hydroxide was used for the synthesis of IM-12. In both cases, the Si/Ge molar ratio was relatively low: 8.5 and 4.5 for ITQ-15 and IM-12, respectively. In the following studies,[73–76] **UTL** was found to be preferentially formed under low Si/Ge ratio, equal to 2, in the reaction mixture and in the absence of F^- anions. Highly crystalline **UTL** can be formed using at least 21 different organic SDAs (spiro-azo compounds) under appropriate reaction mixture compositions.[73,74] For possible utilization of extra-large-pore **UTL** in catalytic applications, it was necessary to introduce the active centres by incorporation of tri-valent or tetra-valent heteroelements into its framework. The influence of diverse synthetic parameters such as gel composition, pH of the gel, crystallization time, *etc.* on the selective formation of the **UTL** phase and the content of three-valent heteroelements (B, Al, Ga, Fe and In) was systematically studied.[76]

Generally, germanium is well known to stabilize the formation of double-four-ring units (D4Rs) and to be preferentially located within them.[77–80] Zeolite **UTL** is not an exception; germanium atoms in **UTL** almost exclusively occupy T-sites in the D4R units forming supportive 'pillars' for pure silica layers

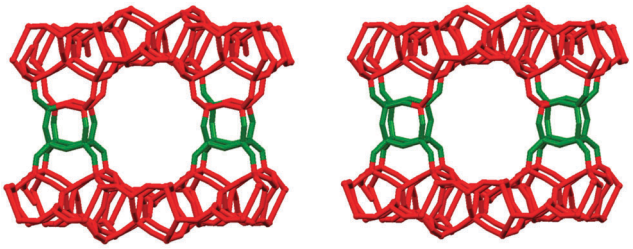

Fig. 1 The schematic view of the germanium location in D4R units between the layers. Ge–O bonds are marked in green colour and as described in the text are susceptible to hydrolysis. Si–O bonds are highlighted in red colour.

consisting primarily of 5-rings. This is a characteristic feature of germanosilicate zeolites, which can be found also in other zeolites, for instance **IWW**[81] or **ITH**.[82] The chemical composition of **UTL** prepared from reaction mixtures with a Si/Ge molar ratio of 2 can vary in the final solid in the 4.3–6.0 range. For the molar ratio Si/Ge = 4.3, this translates into an average of 7 Ge atoms per each D4R unit, [7Ge,1Si] (Fig. 1). The upper limit (Si/Ge = 6.0) gives an average composition of D4R units as [5Ge,3Si]. This means that until the Si/Ge ratio is equal to 6 one of the 4-rings in the D4R consists entirely of germanium atoms while the remaining one is of a mixed occupancy.[83] This regioselectivity of the Ge atoms that occurs in the assembly step is important for understanding the subsequent disassembly step.

The substitution of germanium into the silica framework can strongly affect the hydrothermal stability of a zeolite. It was reported by Li and coworkers that zeolites become increasingly unstable in water with an increasing content of germanium.[84,85]

4. The disassembly step

Substituted-**UTL** with its extra-large pore channel system was investigated in many catalytic reactions.[86–88] However, its overall stability has been questionable as under certain reaction conditions the framework appeared to be irreversibly damaged, especially in the presence of water.[89] Indeed, the calcined **UTL** sample undergoes slow degradation when exposed to atmospheric moisture. The first controlled degradation of the **UTL** framework was reported in 2011.[62] Calcined **UTL** was brought into contact with dilute acidic solutions resulting in a profound change in its X-ray powder diffraction (XRD) pattern (*vide infra*), suggesting the formation of a layered material (Fig. 2). It was concluded that germanium bonds such as Si–O–Ge or Ge–O–Ge (preferentially located within the D4R units) were selectively hydrolysed whereas the bonds within the layers, predominantly Si–O–Si bonds, were largely unaffected (Fig. 1). The resulting layered material was designated IPC-1P, Institute-of-Physical-Chemistry (P for Precursor). In essence, when the Si/Ge ratio is low enough, the germanium rich D4Rs are removed from the parent zeolite, which 'unzips' the framework. The resulting IPC-1P layers have a thickness of approximately 9 Å and possess

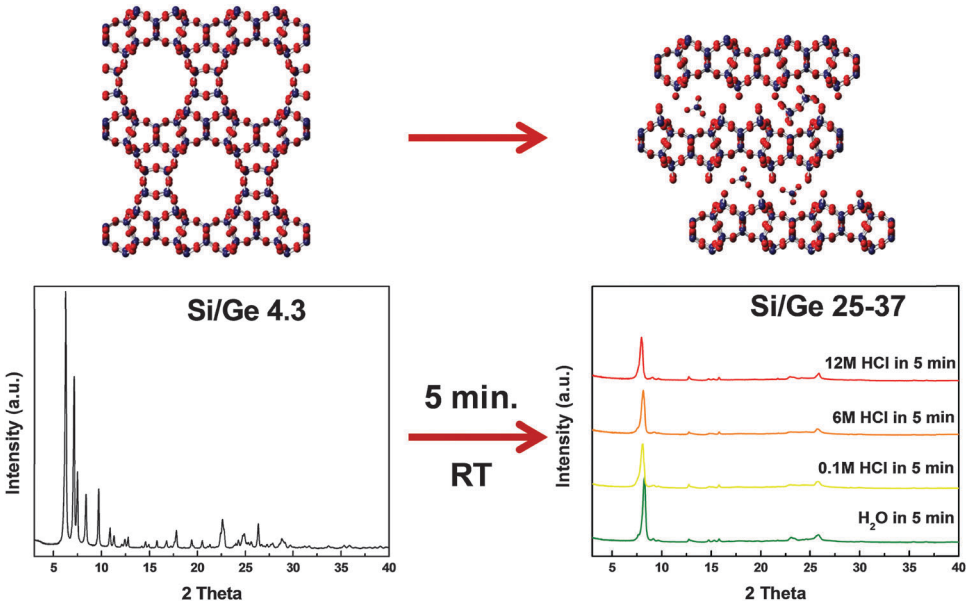

Fig. 2 A schematic description of the disassembly of zeolite UTL (with a Si/Ge ratio of 4.3) *via* hydrolysis in solutions of various acidic conditions for 5 minutes at room temperature. Note that the resulting XRD patterns of the recovered materials show only very slight differences between each other, indicating that the disassembly step is essentially independent of acidity on this time scale.

the same *x*–*y* projection as those of zeolite **FER**, although in the *z*-direction they have a more complicated connectivity corresponding to a longer repeat unit, *i.e.* 12.5 Å *vs.* 7.5 Å.[19] Similar to the ferrierite precursor (preFER), IPC-1P consists of rigid, compact layers that possess neither intra-layer zeolite-like channels nor well-defined inter-layer pores.[90]

In order to control this disassembly process it is important to understand what is happening during the process as a whole. The mechanism of ADOR was studied in detail on calcined zeolite **UTL** samples with a Si/Ge ratio in the range of 4.3–6.0 corresponding to at least 5 Ge atoms in each D4R unit (discussion *vide supra*, Fig. 1). The conditions were chosen to investigate the effect of acid strength of the hydrolysis solution on both the mechanism and products formed, from pure water up to 12 M HCl. This included stopping the hydrolysis after 5 minutes at ambient temperature. The solids recovered after 5 minutes of hydrolysis in solutions of different acidity at ambient temperature do not show any sign of unhydrolysed **UTL** (Fig. 2). Their powder XRD patterns are very similar to each other, independent of the acidity of the solution. Solid-state ^{29}Si magic-angle spinning nuclear magnetic resonance (MAS-NMR) of samples hydrolysed at ambient temperature showed very similar spectra containing majority of Q^4-signals but also some Q^3- and a minor amount of Q^2-type Si atoms from the hydrolysed D4Rs.[91] The chemical composition rapidly changes after 5 minutes of hydrolysis as the Si/Ge ratio increases for all samples into the range 26–37. Based on these findings, the hydrolysis step is considered to be an extremely fast process. It proceeds independently of the acid concentration extracting most of the Ge atoms that are preferentially located within the D4R unit. Solution-state NMR of the hydrolysis solution indicates the presence of dissolved silicate species, indicating the loss of not only the Ge, but also Si from the D4R units.

The structural changes occurring during the hydrolysis of **UTL** were primarily characterized by X-ray powder diffraction followed by sorption analysis (Fig. 2). The main indicator of these structural changes is the position of the inter-layer 200 reflection corresponding to the thickness of the layer plus the inter-layer separation. After hydrolysis, the contraction of the inter-layer space is reflected by a shift of the 200 reflection from 6.15° 2θ to ~8.0–8.5° 2θ, corresponding to a *d*-spacing of 14.4 and 10.4–11 Å, respectively, indicating a contraction of the inter-layer space by about 4 Å. This is consistent with the removal of the entire D4R units (silicon and germanium) from the inter-layer space, which obliterates the channel system and is demonstrated by the much reduced sorption capacity of IPC-1P (both as-synthesized and calcined) in comparison with the parent **UTL** zeolite.[62,92] The integrity and preservation of the original **UTL** connectivity within layers was confirmed by high-resolution transmission electron microscopy (HRTEM).[92] Moreover, the transformation of **UTL** into IPC-1P can be monitored also by Atomic Force Microscopy (AFM).[93] The measured step heights in **UTL** and IPC-1P (estimated as 14 and 10 Å, respectively) were closely related to changes in d_{200}-spacing found for **UTL** and IPC-1P by XRD (14.4 and 10.6 Å, respectively). AFM also revealed that the layers remain intact and undamaged after hydrolysis supporting the idea of the framework being disassembled without solution-mediated recrystallization of the layers.[93]

5. The organisation step

Once hydrolysis has occurred the next step can be organisation of the layers in such a fashion that they can be further directed into new materials. If one simply attempts to reassemble the

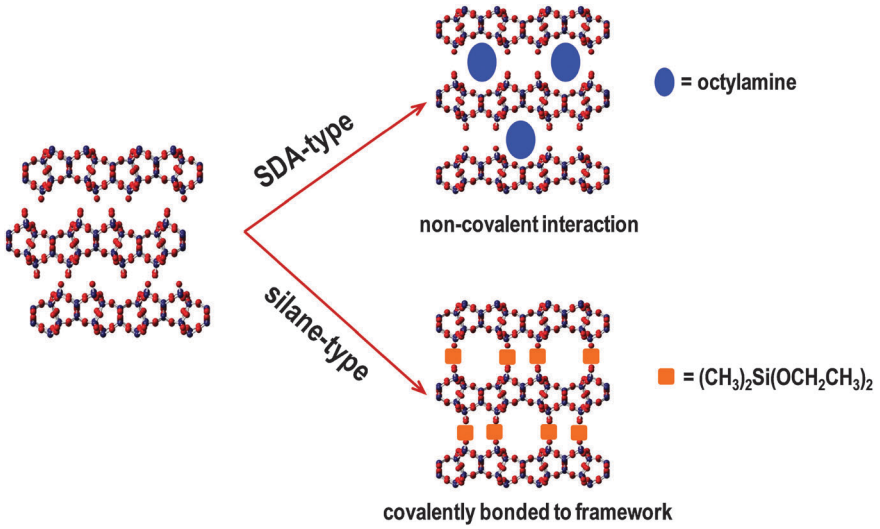

Fig. 3 Two methods for organising the layers of IPC-1P into arrangements suitable for reassembly into crystalline materials *via* the intercalation of species that act as SDAs or are covalently bonded to the framework.

zeolite directly by calcination of the direct product of hydrolysis (after 5 minutes at room temperature) one invariably obtains a poorly ordered material denoted as IPC-1 where the layers are thought to be partially connected and partially collapsed onto each other,[62] producing a material referred to as sub-zeolite.[59,94] This suggests that directly after hydrolysis the layers are not yet properly organised to condense into a crystalline material. The next step in the ADOR process is therefore to organise these layers into an orientation that can easily form a new, highly crystalline material. Research has shown two basic mechanisms by which this organisation can occur.

(i) Intercalation of an organising agent, either an SDA-type organic that orders the layers through non-covalent interactions or species that will end up being covalently incorporated into the final framework (*e.g.* a silicon-containing organising agent, Fig. 3).

(ii) A self-organisation of the layers that occurs on heating under certain conditions. This type of process can have two possible outcomes that depend on the conditions used.

(a) De-intercalation of any residual species remaining between the IPC-1P layers together with an alignment of the layers.

(b) Rearrangement of the silica within the layers to build layers of different structures to IPC-1P that are suitably organised for condensation into a new material.

5.1 Intercalation of an organising agent

IPC-1P layers have a dense grid of silanol groups on the surface formed after the degradation of the D4Rs arranged in groups of four, which we call silanol quadruplets.[95,96] These silanol quadruplets on the face of adjacent layers are available for interaction and eventually condensation forming new connections between the layers.[96] The key to the organisation step is therefore to arrange the layers so that these silanol quadruplets are in the correct position to condense into a reassembled material. The silanol groups from adjacent layers can condense forming new connecting units, oxygen bridges, producing a novel 3-dimensionally connected ordered framework, denoted as IPC-4, being assigned the structure code **PCR** by the International Zeolite Association (IZA).[63]

Once the layers are properly positioned with respect to each other, surface silanols are adjacent to each other and their full condensation is favourable. It appears, based on the success of the procedure that the intercalation of appropriate organics like amine or quaternary ammonium cations in between the layers, *e.g.* octylamine, triethylamine, dipropylamine, trimethylphenylammonium cation, plus ionic liquids such as 1-methyl, 3-ethyl imidazolium[63,97] favours congruent condensation. Organic molecules appear to help organisation of the layers as mentioned above and the following reassembly step results in the formation of the three-dimensional crystalline framework of IPC-4 (**PCR**) possessing 10- and 8-ring channels with pore diameters 5.8 × 3.8 Å, and 4.5 × 3.6 Å, respectively (Table 1).[63] The original Ge-D4R units in **UTL** are replaced by individual simple oxygen bridges in IPC-4, which reduces the pore diameters.

Alternative types of intercalating agents that can be used to organise the layers in IPC-1P are those that can end up covalently bonding to the framework. A good example of this type of compound are alkoxysilanes, typified by diethoxydimethylsilane, $(CH_3)_2Si(OCH_2CH_3)_2$. Intercalation of this material onto the layers helps to organise them through condensation of the $Si(CH_3)_2$ units on the silane with the silanol groups on the IPC-1P layers. In the organised materials the two methyl groups on the added silane remain unreacted under the conditions used for the organisation step (as can be shown using solid-state nuclear magnetic resonance, NMR). However, the great advantage of the ADOR process for zeolites with D4Rs connecting the layers (or layers having silanol quadruplets) over other approaches using directly synthesised layers is that these $Si(CH_3)_2$ groups are geometrically pre-disposed for further reaction, so that these layers can end up forming a true zeolite

Table 1 The overview of pore-diameters of the channel system in the parent **UTL** zeolite and all novel zeolites prepared by the ADOR method to date. The red part in the structure marks the silica layers and the blue part highlights the connecting units of the layers

	Channel size					
Structure type	14-ring (nm)	12-ring (nm)	12-ring (nm)	10-ring (nm)	10-ring (nm)	8-ring (nm)
UTL 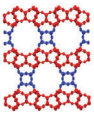	0.95 × 0.71	0.85 × 0.55	—	—	—	—
IPC-7 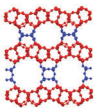	0.95 × 0.71	0.85 × 0.55	0.66 × 0.62	0.54 × 0.53	—	—
IPC-2 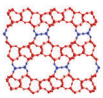	—	—	0.66 × 0.62	0.54 × 0.53	—	—
IPC-6 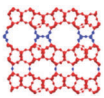	—	—	0.66 × 0.62	0.54 × 0.53	0.58 × 0.38	0.45 × 0.36
IPC-4 	—	—	—	—	0.58 × 0.38	0.45 × 0.36

on reassembly – something that is not possible using directly synthesized layers, which do not have similar silanol quadruplets.

5.2 Self-organisation

Under appropriate conditions, there is no requirement for additional intercalating species to organise the IPC-1P layers because they will self-organise. This process involves heating the system to 85–100 °C for around 24 hours. Under neutral or mild acid conditions (0.1 M HCl) the inter-layer spacing, as assessed using the 200 reflection, progressively shifts with time to lower inter-layer distances from 8.27° to 8.5° 2θ (d_{200}-spacing 10.7 to 10.4 Å) while losing even more Ge atoms from the framework (Si/Ge increases with time to approximately 100 after 24 hours), see Fig. 4. This is a de-intercalation process as it leads to the removal of any remaining hydrolysed species from the inter-layer space, which consequently contracts slightly. The reassembly of the solid into a 3-dimensional material by calcination forms the IPC-4 (**PCR**) zeolite.

On the other hand, hydrolysis in a highly acidic solution (12 M HCl) implies another mechanism. Over the next hours (8, 16 and 24 hours) the crystallinity gradually returns and inter-layer reflection 200 gradually shifts to lower 2θ values (7.7° 2θ), *i.e.* to a longer inter-layer distance with a d_{200}-spacing of about 11.5 Å (Fig. 4). Highly-acidic hydrolysis conditions induce the rearrangement process where any remaining framework species from D4R units are removed while new Si–O–Si bonds are created forming a single-four-ring-precursor, which is condensed into complete single-four-ring (S4R) unit during calcination. As there is not enough silicon atoms from hydrolysed D4R units to complete the new S4R unit, we suppose that silicon atoms from intra-layer T positions migrate in between the layers, which is enabled by highly acidic conditions or it is simply some residual silica, which is expected to be present in any such preparation (*e.g.* precipitating when the synthesis mixture cools to room temperature). Such migration of tetrahedral silicon species has recently been seen by Hong and co-workers in the zeolite natrolite[98] and for the healing of defects in zeolite YNU-2.[99] As a result, this process removes the vast majority of Ge atoms producing high Si/Ge ratios (greater than 200). Calcination of the material leads to IPC-2 zeolites that possess the same connectivity as zeolite **OKO**. Generally, the highly acidic condition promotes the making/breaking of Si–O bonds following the reaction pathway.[100] It should be noted that the level of sample washing after hydrolysis can affect the amount of residual Si needed for building novel connections. In other words, proper washing in order to reach neutral pH can remove some of the newly created bonds. It will result in a defected structure after reassembling. Therefore, it is recommended to wash just roughly the solid after hydrolysis independently of the used acidic solution.

6. The reassembly step

The final step in the ADOR process is to take the organised precursor layers and reconnect them. This reassembly process occurs through heating of the sample (calcination) to temperatures in excess of 500 °C. Taking any of the organised solids and calcining them leads to fully connected zeolites, either IPC-4 (for layers connected simply through an oxygen atom) or IPC-2 for layers connected through a S4R.

The phenomena of direct connection of layers has been reported for other layered zeolite precursors, *e.g.* MCM-22P, preFER, where calcination leads to a condensation of the layers *via* surface silanols forming a complete three-dimensional

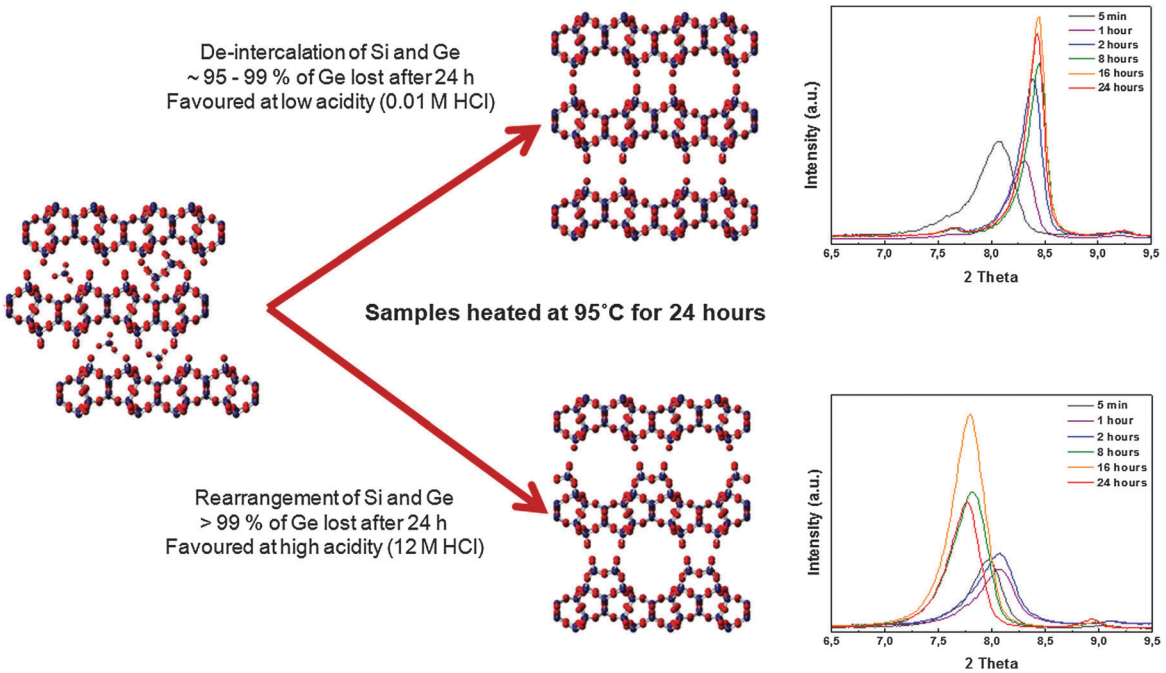

Fig. 4 Schematic diagrams of the acidity-dependent self-organisation processes that occur during the heating of IPC-1P in contact with solutions of 0.01 M HCl (bottom) and 12 M HCl (top). The effect of the rearrangement in 12 M HCl is an increase in interlayer spacing – the position of the 200 reflection moving to a lower 2θ angle, while that of the 0.01 M HCl is a shift to a higher 2θ angle, indicating a decrease in interlayer spacing.

crystalline framework, **MWW**[32] and **FER**,[90] respectively. There are other examples when calcination of layered zeolite precursors may result in less ordered frameworks, for instance, layered NU-6(1) and EU-19 have the same **NSI** topology, however, only in the case of NU-6(1) a three-dimensional zeolite ordered **NSI** topology is formed after calcination.[94] By calcination of EU-19 one can get a material denoted EU-20b with still unresolved structure.[101] Even more interesting is the case of layered silicates containing ferrierite-type layers. There are many such materials that were obtained using different organic SDAs producing various arrangements of the layers relative to each other, *i.e.* with different shifts along *a* and *c* axis.[102,103] Topotactic condensation of these layered materials leads to zeolites **FER** or **CDO** type (see discussion in following chapter), or to poorly ordered framework silicates. Marler *et al.*[103] suggested that the quality of the final material may depend on many factors like: (i) the distance of terminal silanol or silanolate groups because a distance of less than 4 Å can lead to intra-layer condensation rather than the inter-layer one; (ii) the presence of silanol defects, which causes a random inter-layer condensation; (iii) the formation of inter-layer hydrogen bonds considering their stabilizing effect – keeping the layers at the appropriate positions in the structure; (iv) the stacking disorder (randomly varying shift vectors); and (v) the type of intercalated organic cation (used as a SDA for the synthesis).

The D4Rs can also be replaced by another connecting unit, a single-four-ring (S4R). Alkoxysilylation of layered precursors like MCM-22P (**MWW** topology), preFER (**FER**), or CDS-1 (**CDO**) leads to the so called interlamellar expanded zeolites (IEZ).[104] They have enlarged pore windows in comparison to their three-dimensional parent forms, however, as per definition they are not zeolites.[104–106] New silica bridges between layers have only two tetrahedral neighbours plus OH or other groups and thus IEZ are not strictly zeolite frameworks. IPC-1P is different regarding the location of surface silanols as residues after D4R removal because of their arrangement in a quadruplet. During alkoxysilylation with diethoxydimethylsilane, two ethoxy groups in one silane molecule connect to the opposite layers *via* the reaction with surface silanols. The methyl groups of the silanes, which are initially present, are converted to geminal silanols upon heat treatment and, being close enough, they enable the formation of Si–O–Si bonds in the plane forming new S4R units sandwiched between the layers. The resultant material has a 3-dimensionally connected framework fulfilling the conditions for being recognized as a zeolite. This zeolite was denoted as IPC-2.[62,63] The smaller size of its connecting unit (D4R *vs.* S4R) results in a decrease in the pore diameters to 12- and 10-ring, 6.6 × 6.2 Å and 5.4 × 5.3 Å, respectively (Table 1).[63] ^{29}Si solid state NMR confirmed only a negligible amount of Q3 signals coming from uncondensed silanols for both IPC-4 and IPC-2 zeolites.[63]

7. ADOR kinetics and control over porosity

The self-organisation processes described in Section 5 shows that there are two different processes occurring during this new synthetic route; de-intercalation and rearrangement. The two outcomes are favoured by different conditions; low acidity

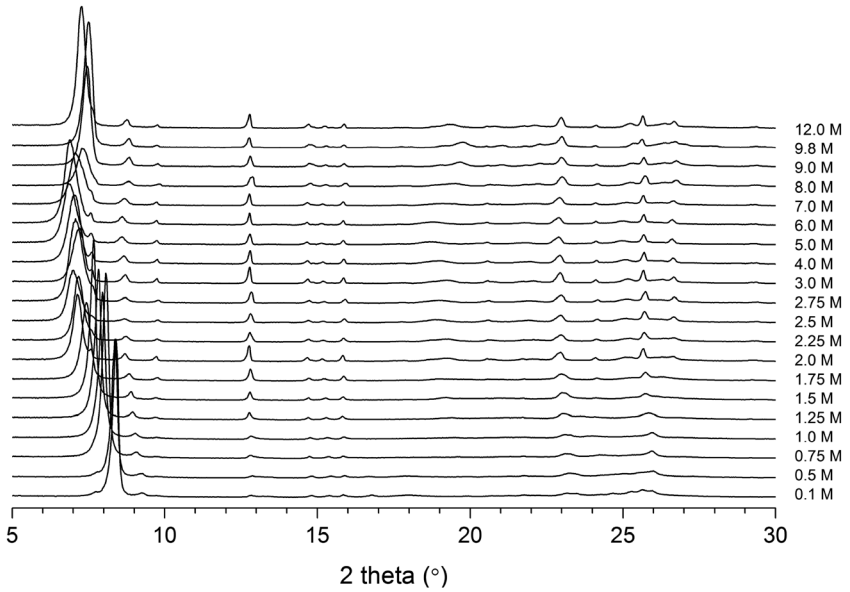

Fig. 5 Powder X-ray diffraction patterns with the varying molarity of HCl solution.

conditions favour the de-intercalation route and final reassembly into IPC-4 (**PCR**), while high acidity favours the rearrangment process and the synthesis of IPC-2 (**OKO**) on reassembly. It is clear that the rates of these two processes are the controlling factors. The rearrangement can still take place at low acidity, but it is slow compared to the de-intercalation, whereas at higher acidity the rate of the rearrangement process is significantly enhanced.

The question asked at this stage was – can any form of control be imposed on these processes by governing their rates and imposing the control over the final products? What happens if the rates of the de-intercalation and rearrangement processes are approximately equal? It was found that intermediate conditions of these extremes (*i.e.* molarities between 0.01 M and 12 M) lead to some exciting chemistry occurring during the ADOR process of **UTL** and that different zeolite structures could be formed.

Samples of calcined **UTL** were heated at 95 °C up to 17 hours in a range of varying acidities in the hydrolysis solution (from 0.1 M to 12 M) and then calcined (Fig. 5). It was found that above 7 M the product formed was predominately IPC-2[91,107] although there was an increasing degree of disorder present in the final materials as the molarity was decreased from 12 M. This disorder was attributed to the existence of different species between the layers (*e.g.* oxygen bridges, S4Rs and D4Rs) and a possible lateral movement of the layers with respect to one another. Very low acidic conditions (neutral – 0.1 M) produced IPC-4. When the molarity was further increased new materials were found to form at these intermediate molarities. With increasing $[H^+]$ there was a gradual change in the position of the 200 reflection towards lower diffraction angles, which was indicative of an increase in the inter-layer space (as measured by d_{200}). There is a linear relationship between the molarity of the hydrolysis solution and d_{200} as the concentration increases up to 3 M (Fig. 5). Above this molarity there is a slightly more complex relationship whereby d_{200} passes through a maximum at 5 M then decreases again as the concentration increases to 7 M where it then remained approximately constant up to concentrations of 12 M.[91]

The change in d_{200} with molarity is also mirrored by the nitrogen adsorption data of the calcined product (Fig. 6). The BET areas and pore volumes show a linear relationship up to 3 M, then pass through a maxima at 5 M before decreasing to 7 M where it largely remains constant. With the aid of TEM, these observations were explained by considering the species that were present between the layers, *e.g.* oxygen bridges, S4Rs or D4Rs. For IPC-4, there are only oxygen bridges between the layers, whereas in IPC-2 there are S4Rs present between the layers resulting in an increased d_{200} and porosity values (9.1 *vs.* 11.8 Å, 151 *vs.* 480 $m^2\ g^{-1}$ and 0.06 *vs.* 0.18 $cm^3\ g^{-1}$, respectively). The linear relationship observed in the d_{200} and adsorption plots can be attributed to the quantity and type of inter-layer connections. The value of d_{200} and porosity values, like the BET surface area or the total pore volume, increase with the increasing molarity, which can be attributed to an increased proportion of S4R connections. The increased S4R connections is a consequence of the increased rate of the rearrangement process with increasing acidity, leading to products with successively greater numbers of S4R connections as acidity is increased.

There is a special situation at a molarity of 1.5 M where the rates of de-intercalation and rearrangement are equal leading to a final material that possesses the same quantity of oxygen bridges and S4R connections. The material was named IPC-6 and on average the unit cell contains one each of the different types of connections leading to a material that has 12-10 and 10-8-ring pore systems (see Scheme 1 and Table 1).[91] The proposed structure of IPC-6 was found to be a good fit for the

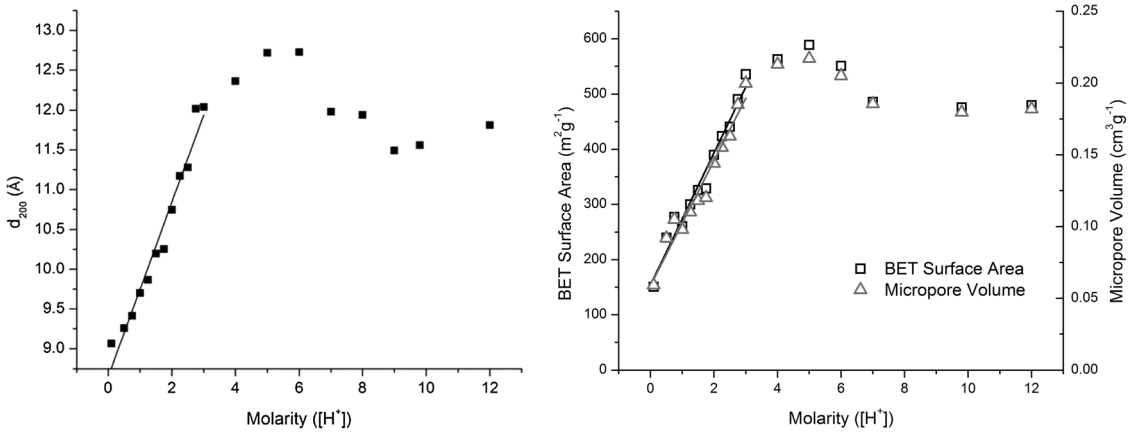

Fig. 6 The dependence of the 200 position (on the left) and surface area/micropore volume (on the right) on the acidity (measured in molarity).

experimental data and a Rietveld refinement using synchrotron data was successfully completed. The two different inter-layer spacings, 11 Å for S4R connections and 9 Å for oxygen bridges, were also confirmed by TEM, see Fig. 7. Moreover, IPC-6 has the Si/Ge ratio around 44 confirming that most Ge atoms were washed out of the system. A similar model can be used for the maxima observed at 5 M where the layer connections consist of an equal quantity of S4Rs and D4Rs. The material was named IPC-7 and again the unit cell consisted of one each of these connections to give a material with 14-12 and 12-10-ring pores (Table 1).[91] The proposed model matched the experimental data except that a successful Rietveld refinement could not be obtained due to the local disorder present in the material as observed by TEM (Fig. 7). The low germanium content in IPC-7 (Si/Ge molar ratio 76, *i.e.* approximately 1 Ge atom per unit cell) confirms that the present D4R units are not residues from parent **UTL** and hence the rearrangement process has to take place to create novel Si-D4R units. As the molarity increases past 5 M, the d_{200} value decreases and becomes approximately constant from 7 M and above where IPC-2 is formed.[91]

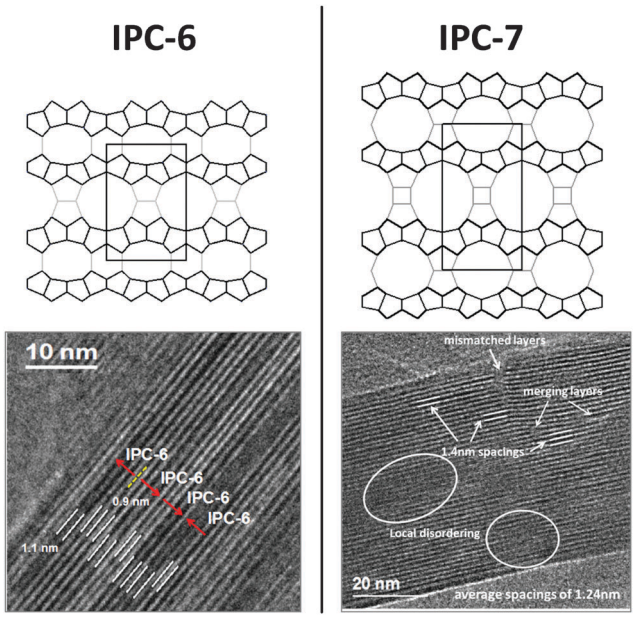

Fig. 7 Structures of IPC-6 and IPC-7 showing their differing inter-layer connectivities (colored grey). Representative TEM images of IPC-6 and IPC-7 showing the difference in inter-fringe distances caused by the disorder stacking of the materials.

Overall, the *d*-spacing of the final materials increases proportionally with the increasing acid concentration in the range from 0.01 M to 5 M as it is demonstrated in Fig. 6. Under specific concentrations we obtain well-ordered zeolites with increasing *d*-spacing in line IPC-4 (0.01 M) < IPC-6 (1.5 M) < IPC-2 (3 M) < IPC-7 (5 M). Above 5 molarity the final solids mostly with IPC-2 topology are more or less disordered as it was discussed above.

The control of the de-intercalation and rearrangement processes allows for continual linear control over the porosities and pore volumes of the final zeolite materials. It can be simply achieved by choosing appropriate molarity for the hydrolysis solution which can result in delivering surface areas in the range of 150–590 $m^2\ g^{-1}$ and pore volumes of 0.06–0.22 $cm^3\ g^{-1}$ for the final material (Fig. 8). This degree of control has never been witnessed in zeolite chemistry before. In fact, the only way to alter the porosity previously was to synthesize different framework topologies which did not yield fine control over the final properties. Here it is achieved by controlled treatment enabling almost ''continuous'' replacement of layers with D4R units by those having S4Rs or simple oxygen bridges.

The stability of the parent zeolite **UTL** with high Ge content is rather poor; the structure collapses in time when it is left exposed to the laboratory atmosphere. The incorporation of germanium creates a degree of hydrolytic instability, which many large pore zeolites may suffer from (*e.g.* **ITV**, **ITT**, **IRY**, **IRR** *etc.*). The ADOR method has been shown to utilize this inherent instability and use it to its advantage creating new zeolites that contain very little germanium and their stabilities are greatly enhanced. This has been used to create the medium/large pore zeolite IPC-2 (12-10-ring and 10-8-ring pore systems) and the large pore zeolite IPC-7 (14-12-ring and 12-10-ring pore systems), see Table 1.

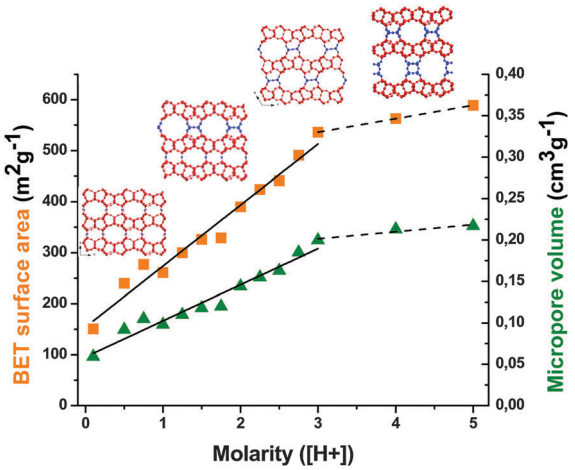

Fig. 8 Relationships between the BET surface area (left-hand axis, orange squares) and the micropore volume (right-hand axis, green triangles) under hydrolysis conditions, showing how porosity is continuously tunable.

One may ask, what is the effect of basic solutions on the stability of the **UTL** framework? According to general experience/knowledge, highly basic solutions cause a non-selective dissolution of a zeolitic framework. For **UTL** water solutions of tetramethylammonium hydroxide (TMA–OH) of pH 9 and pH 12 were tried. Highly concentrated TMA–OH solution (pH 12) just confirmed the expectations of zeolite dissolving. However, under pH 9 de-intercalation occurs, which finished within two hours in a typical IPC-1P material. Nevertheless, a prolongation of the hydrolysis time (8–24 hours) showed significant turn in the mechanism as it led to a typical IPC-2 material with S4R units between the layers, *i.e.* rearrangement prevailed. In other words, the first hours of hydrolysis under pH 9 were similar as under pH 7, afterwards basic solution initiated the rearrangement processes.

These data clearly evidence that there is significantly different stabilities of Ge–O bonds in comparison with Si–O bonds. The Si–O bonds withstand the pH around 9 and below (in short term) while Ge–O bonds break almost immediately under these conditions. In fact, this is the most important prerequisite of the ADOR process, when zeolites with appropriate topologies and chemical compositions are available.

8. Layer manipulation

The organisation of two-dimensional (2D) layered materials is critical for the outcome of the reassembly procedure (calcination) as only appropriately ordered layers can lead to a regular 3D zeolites upon condensation. It is therefore essential to understand the inter-layer interactions at the atomistic level. Due to experimental difficulties in obtaining sufficient atomistic details for majority of layered zeolites the involvement of computational chemistry is rather beneficial. Computational studies relevant for layered zeolites were recently reviewed as a part of more comprehensive review on layered materials.[35] The following section is focused on a computational description of layered materials relevant for the ADOR process.[95,96,108–110]

The ADOR protocol has been described for **UTL** zeolites that has been transformed into two new zeolites (**PCR** and **OKO** topologies) *via* the IPC-1P layered intermediate.[63] From the experimental powder XRD of the IPC-1P layers the spacing of about 10.7 Å has been determined,[62] however, a detailed insight into inter-layer interactions could not be deduced from experimental data because of the low crystallinity of the material itself. The atomistic details of interacting IPC-1P layers were therefore investigated computationally.[96] The calculations were performed with the periodic model consisting of two interacting IPC-1P layers at the density functional theory (DFT) level. A large variety of possible inter-layer arrangements, corresponding to various local minima on the potential energy surface, has been reported. All arrangements show a large number of inter-layer hydrogen bonds (H-bonds) as a consequence of a high density of silanols on the IPC-1P surface (2.3 OH nm^{-2}). The surface of the IPC-1P layer is depicted in Fig. 9, the quadruplets of surface silanols result from the hydrolysis of D4R units connecting the layers in the "parent" **UTL** zeolite. The distance between the silanols within the quadruplet is about 5 Å and even the distance between the silanols of different quadruplets is only about

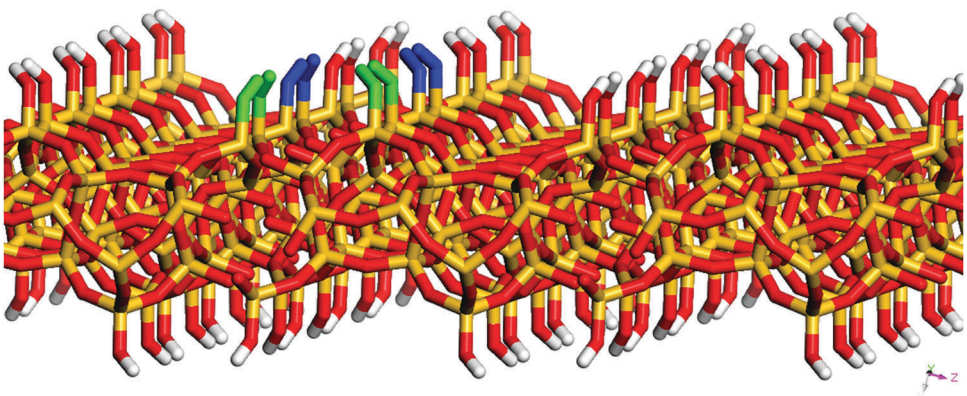

Fig. 9 Surface of the IPC-1P layer showing a large density of surface silanols grouped into surface "quadruplets"; examples of silanol quadruplets are depicted in green and blue. Silicon, oxygen and hydrogen atoms are depicted in yellow, red, and white colours, respectively.

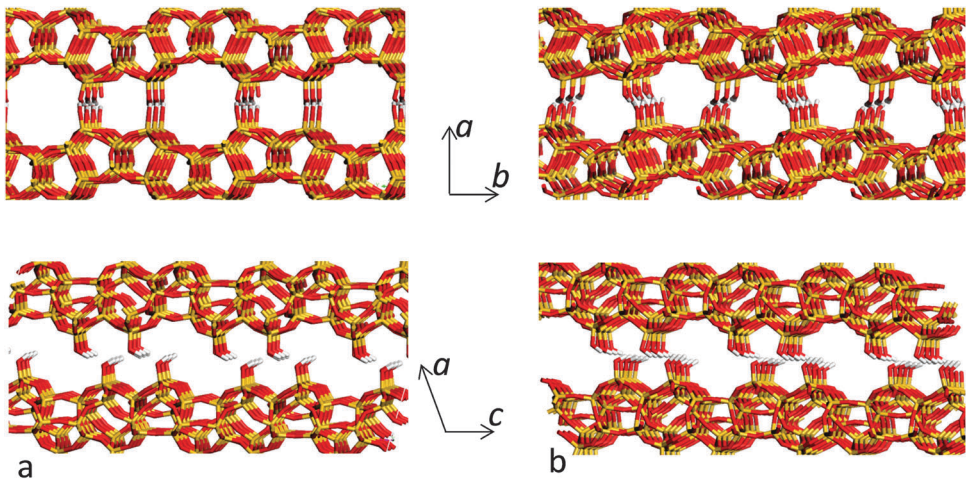

Fig. 10 Inter-layer H-bond networks formed along the ac plane without (a) and with (b) an inter-layer shift. Interacting silanol quadruplets forming six H-bonds can be seen in the lower part of the figure (see Fig. 9 caption for colour scheme).

7.3 and 8.5 Å along the *c* and *b* unit cell (UC) vectors, respectively (using the UC vectors defined for the parent **UTL** zeolite). Following the classification of Ugliengo[111] all these surface silanols are isolated and they cannot be involved in the formation of any significant intra-layer H-bonds. The situation is quite different when considering interacting IPC-1P layers – distances between silanols are suitable for the formation of inter-layer H-bonding networks (Fig. 10). The strength of the inter-layer interaction correlates with the number of inter-layer H-bonds; the most favourable arrangements show the maximum number of inter-layer H-bonds (six for a pair of silanol quadruplets on adjacent surfaces, Fig. 10). Surface silanols are on average involved in 1.5 H-bonds (25% silanols acts as acceptors, 25% silanols acts as donors, and 50% silanols are involved as both proton donors and proton acceptors in the same time). An inter-layer H-bond has an average strength of 21 kJ mol^{-1}. Inter-layer dispersion is significantly less important, it accounts only for about 26% of the overall interaction energy.

The inter-layer arrangements were classified based on the lateral shifts of adjacent layers; the H-bonding network can be formed between silanol quadruplets resulting from the hydrolysis of particular D4R units without a lateral shift (Fig. 10a) or a H-bonding network can be formed between different silanol quadruplets upon the shift along *b* or *c* vectors (Fig. 10). The most stable arrangement was found for unshifted layers with H-bonding networks parallel to the *ac* plane, characterized by an interaction energy of −43 kJ mol^{-1} OH^{-1} corresponding to an adhesion energy of 1 kJ mol^{-1} $Å^{-2}$. Laterally shifted arrangements are about 2–3 kJ mol^{-1} OH^{-1} less stable. Note that different arrangements of layers could give rise to different inter-layer connectivities (Fig. 10) upon calcination, see the discussion below. The role of the structure directing agent (SDA) in the relative energies of various inter-layer arrangements was also investigated;[63] the energy difference between the unshifted and shifted arrangement increased due to the presence of octylamine molecules in between IPC-1P layers. It should be noted that all computational investigations discussed above assumed that the surface consists of isolated silanols only (no silanolates). While this is a likely relevant model for the acidic or neutral environment the involvement of silanolate may become important with increasing pH (see ref. 111 for an excellent discussion of this phenomenon).

The high density of surface silanols due to the presence of silanol quadruplets determines the surface properties of IPC-1P and it also leads to various inter-layer arrangements. While such a large density of surface silanols can be found in all layered materials identified as potential candidates for the ADOR process (Table 2), for all the well-known layered zeolites, such as MCM-22P and preFER, the surface silanol density is significantly lower. For instance, a surface silanol density of 1.12 OH nm^{-2} found for MCM-22P is less than half of the silanol density on the IPC-1P surface. The topology of the

Table 2 Properties of two-dimensional (2D) zeolite layers corresponding to the selected three-dimensional (3D) regular zeolites

3D zeolite	2D zeolite	Silanol density [OH nm^{-2}]	*R*(O···O) [Å]	*R*(O···O) [Å]	Layer thickness [Å]	Framework density [TO_2 10^{-3} $Å^{-3}$]
MWW	MCM-22P	1.12	8.31	8.31	25.2	15.9
FER	preFER	1.85	5.99	7.54	9.5	17.6
UTL	IPC-1P	2.30	4.76	5.05	9.1	15.6
IWW	IPC-5P	3.02	4.86	5.00	7.8	16.6
IWV		2.20	4.80	5.09	9.0	15
IWR		2.83	4.91	5.02	7.7	15.6
ITH		3.13	4.82	4.97	7.6	17.4
ITR		3.12	4.96	5.09	7.7	17.4

MCM-22P layers, specifically the lateral mirror plane symmetry, together with the large distances between intra-layer silanol groups (8.3 Å, Table 2) allows only one topologically distinct 3D zeolite (**MWW** structure) upon the full inter-layer condensation. The surface silanol concentration in preFER is between the concentrations reported for MCM-22P and IPC-1P. Because of the absence of mirror plane symmetry within the layer, two distinct inter-layer connectivities can be expected for preFER layers upon condensation (**FER** and **CDO** zeolites).[53] The stacking of **FER** layers was modeled using the CVFF force field and the configurational bias Monte Carlo simulations.[112] Simulations showed that the presence of a cetyltrimethylammonium cation (C_{16}TMA) led to the re-arrangement of individual layers from RUB-36 to a preFER material, which is apparently favoured energetically.

The large density of surface silanols is essential for the inter-layer arrangements and, in addition, it also strongly influences the adsorption properties of 2D zeolites; the adsorption of small molecules on IPC-1P was investigated computationally.[95,109] The adsorption of CH_4, CO_2, H_2O, H_2, and N_2 on IPC-1P was investigated using a modified DFT/CC method[113,114] and Lewis acidity of Li-exchanged IPC-1P (with respect to Li-exchanged parent UTL) was modeled using a ω/r correlation method[115] for adsorbed CO probe molecules. However, the most exciting consequence of a large concentration of surface silanols on the IPC-1P surface is the possibility to arrange adjacent layers in different ways and such different inter-layer arrangements could lead (upon the layer condensation) to four topologically distinct zeolites.[108]

Two-dimensional zeolite layers obtained from the parent **UTL** zeolite by removing the D4R pillars were considered as a building unit and all possible 3D zeolites that can be obtained by condensation of these layers were investigated computationally.[108] The adopted computational strategy closely followed the experimental ADOR protocol: layered zeolite (IPC-1P) was obtained from the parent **UTL** zeolite simply by removing the D4R units (disassembly); various interlayer connectivities were considered (organisation), and geometries of topologically unique 3D structures were fully optimized (reassembly). Calculations were performed at the DFT level of theory (PBE and vdW-DF2 exchange correlation functionals for geometry optimization and single-point energy calculations, respectively) assuming that atom connectivity within the individual layer was unchanged and assuming the same layer connectivity between each pair of layers. Therefore, there are four possible 3D structures obtained by direct condensation of IPC-1P layers (Fig. 11). These new zeolites were denoted as **UTL**-D4R(Sym) following the fact that their structures can be derived from the parent **UTL** zeolite upon the removal of D4R pillars and they were classified according to their symmetry (Sym). Topological analysis (coordination sequences and vertex symbols) shows that all four new zeolites are unique; **UTL**-D4R (*C*2/*m*) zeolite obtained from IPC-1P layers without a lateral shift has a **PCR** topology, confirming the experimental findings described above, while other three zeolites have new topologies that are experimentally unknown and are not predicted computationally so far. The **UTL**-D4R (*C*2/*m*) zeolite has intersecting 10- and 8-ring channels. Shifting the layers along the *b* vector results in the reduction of the channel running along *c* from 10- to 8-ring (zeolite **UTL**-D4R (*Pm*), Fig. 11) while the size of the 8-ring channel along *b* is unaffected. The shift of layers along *c* leads to the reduction of an 8-ring channel along *b* to a 7-ring (zeolite **UTL**-D4R (*P*1), Fig. 11) one. The **UTL**-D4R (*Pm*′) zeolite with the

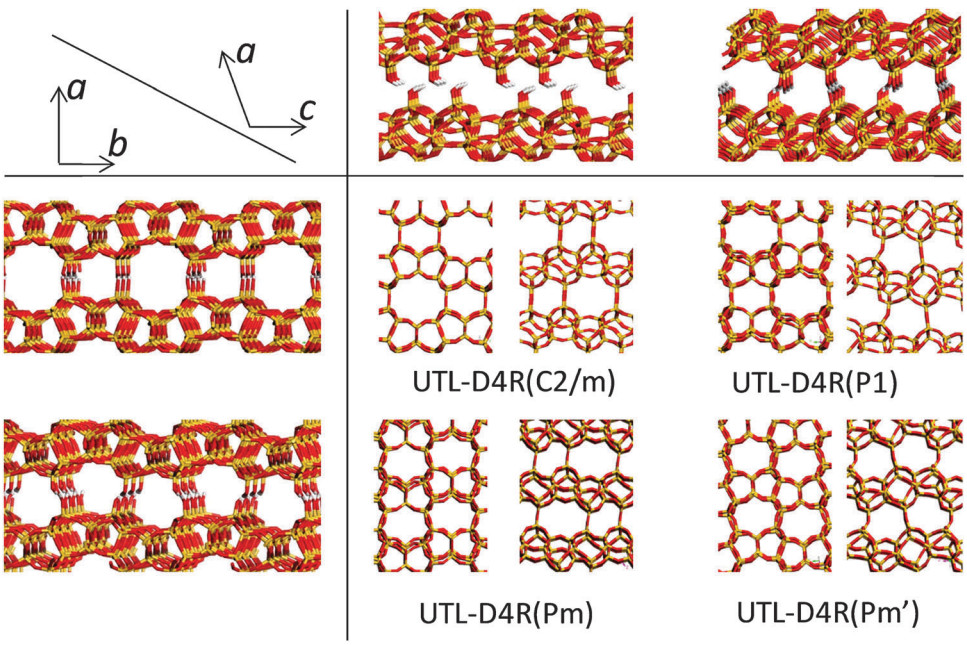

Fig. 11 Zeolites obtained by the direct condensation of IPC-1P layers. Shift of the layers along the b vector starts from 10- to 8-ring channels along *c* and the layer shift along *c* leads from 8- to 7-ring channels along the *b* vector. Four hypothetical zeolites are shown; note that UTL-D4R (*C*2/*m*) is the zeolite IPC-4 with **PCR** code (see Fig. 9 caption for colour scheme).

highest framework energy corresponds to layers shifted along both *b* and *c* vectors. Following the strategy often adopted for characterization of hypothetical zeolites the framework energy with respect to α-quartz,[116] feasibility factors θ,[117] and local interatomic distances (LIDs)[118] were evaluated for zeolites obtained by *in silico* ADOR procedure described above. Zeolites obtained without a shift along *c* satisfy all LID criteria, while those with a shift usually break at least one of the LID criteria.

Structures and properties of three-dimensional zeolites that could be obtained by the ADOR procedure from **UTL** by the introduction of a new S4R unit between the layers were also investigated computationally;[110] the resulting zeolites were denoted **UTL**-SR4(Sym) reflecting the fact that IPC-1P layers are interconnected *via* S4R units (one less than in parent **UTL**). A total of 16 possible interconnections of two IPC-1P layers *via* S4R must be considered; the S4R unit can be connected in four different ways to a lower IPC-1P layer and in four different ways to a higher IPC-1P layer (Fig. 12). Topological analysis (coordination sequences and vertex symbols) revealed that only 8 out of these 16 structures are topologically unique and they have not been reported before. The only exception is the zeolite **UTL**-S4R(C2) that has the **OKO** framework and that is obtained without a lateral shift (Fig. 12). This is the only zeolite among the **UTL**-S4R family that satisfies all LID criteria and has a low feasibility factor.[110] The structure of this zeolite has been obtained based on the powder XRD pattern using the DFT optimized structure as the starting geometry.[63,119] Other zeolites of the **UTL**-S4R family do not satisfy the LID criteria and their feasibility factor is rather high.

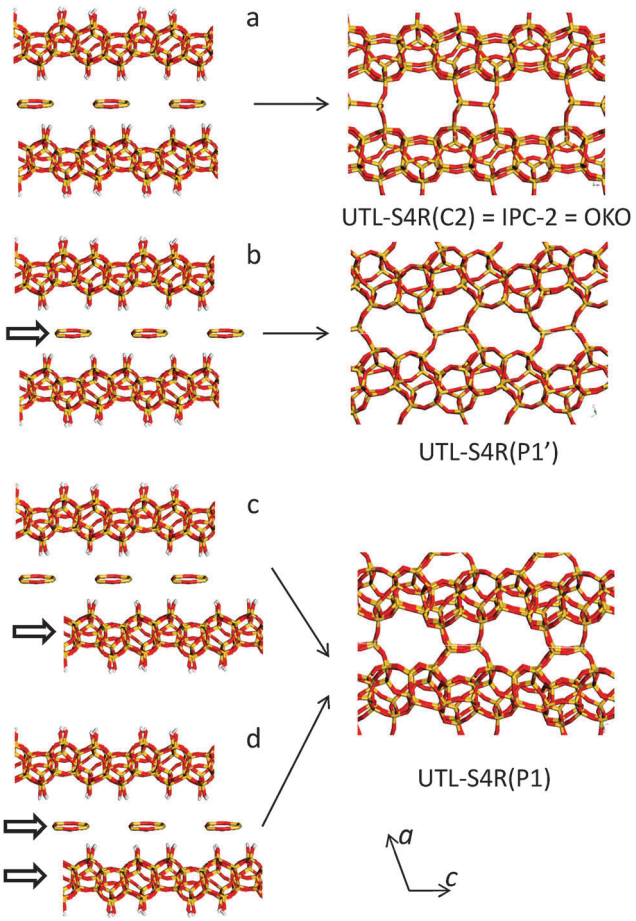

Fig. 12 Connecting the IPC-1P layers *via* S4R units is shown along the b vector direction (considering inter-layer shifts along *c* only). The IPC-1P layer is unshifted and S4R just replaces D4R (a), S4R rings are shifted with respect to IPC-1P layers (b), and first (c) or the second (d) IPC-1P layer is shifted with respect to other IPC-1P layers and S4R. Note that 10-, 8- or 9-ring channels are obtained along *b* in (a), (b), and (c) cases, respectively (see Fig. 9 for colour scheme).

9. Expansion of the inter-layer space

Although this review is dedicated to ADOR as a novel method for the synthesis of zeolites, now we would like to introduce and discuss another aspect of this method regarding its initial top-down synthesis of two-dimensional zeolites. The chemistry of layered materials is very fruitful offering a preparation of many organic–inorganic hydride materials. Here, we will demonstrate its advantage on the IPC-1P layered precursor prepared in the initial step of ADOR.

9.1 Intercalation into IPC-1P

IPC-1P behaves like the majority of layered materials and can absorb other molecules as guests between its layers.[31,120,121] This process, called intercalation, has a special significance with organic guest molecules as they can expand the inter-layer space[122] and allow manipulation of the layers as building blocks with the generation of alternative structures and layer packing architectures. The extreme case, when the layers become separated by large distances (nanometers) and apparently lose contact except *via* the intercalated guest, is referred to as swelling.[31,121,123–125] The layers in as-synthesized IPC-1P are typically cross-linked *via* a dense hydrogen bonding network between surface silanols as elaborated above.[95,96] Thus, two cases of intercalation are encountered: with the preservation of the inter-layer interactions and without, *i.e.* when the bonds are severed. The latter is pre-requisite for swelling of layered zeolite precursors and is best illustrated by the reaction with a long chain surfactants (*e.g.* hexadecyltrimethylammonium cations – $C_{16}TMA^+$), which requires a high pH environment. The major processes associated with the intercalation of organic molecules into IPC-1P and subsequent transformations, which may result in the formation of novel structures, are summarized in Fig. 13. In line with the unofficial convention of naming layered zeolite materials,[59] IPC-1P intercalated with organic molecules can be considered formally as a precursor to zeolite **PCR** (**PCR** precursor) due to its potential for producing this framework upon calcination.

There are numerous zeolite frameworks recognized to produce layered forms.[35,59] Some kinds of organic intercalations have been applied explicitly with several of them, namely **MWW**,[31,33] **FER**,[90] **CDO**,[112] **NSI**,[94] **SOD**,[126] and **RWR**.[127] IPC-1P is the unique layered zeolite material as it is produced by a top-down method from **UTL** and moreover, it has not been

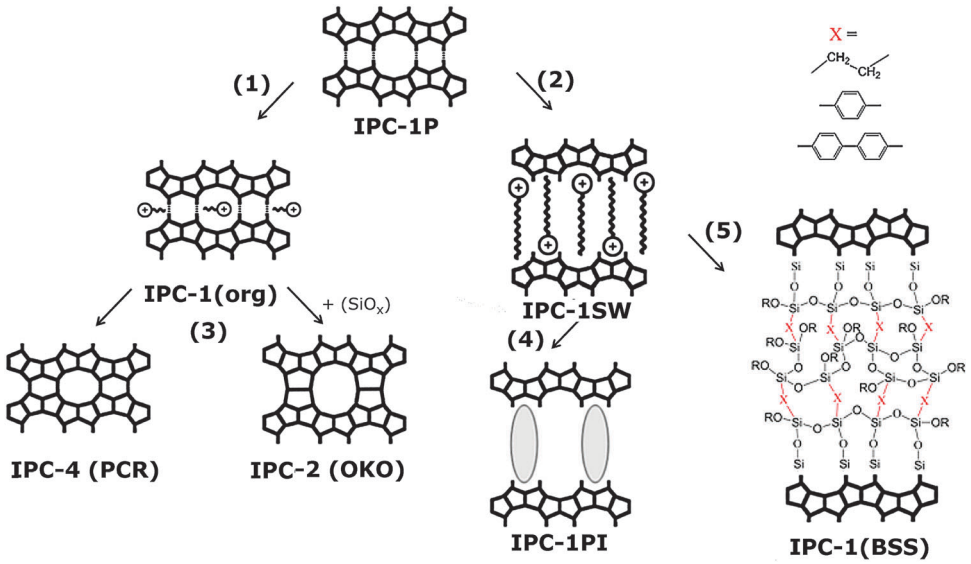

Fig. 13 Post-synthesis modifications of the layered precursor IPC-1P involving inter-layer space manipulation. Steps: (1) intercalation; (2) swelling; (3) calcination; (4) pillaring; and (5) organic linking.

directly synthesized yet. It is further distinguished and unprecedented by its ability to produce another framework **OKO** (COK-14/IPC-2) as the result of formation of S4R bridging units between the layers as already described above.

The study of IPC-1P intercalation focused on the influence of the size and nature of organic intercalating agents on the inter-layer distance in the obtained materials.[62,97,128] The precursor IPC-1P was treated with various amines and quaternary ammonium compounds producing a wide range of inter-layer separations (IPC-1(org), Fig. 13). In many cases, like with amines, there was only a slight layer expansion suggesting preferential horizontal positioning of organic molecules between the dense silica layers. Horizontal intercalation was also concluded in the case of long chain surfactant cations under neutral pH.[128] This can be rationalized due to the constraints on inter-layer expansion by the inter-layer hydrogen bonding. It is apparently holding the layers together and unless broken, *e.g.* at much higher pH as elaborated below, it does not allow real separation. While this type of intercalation is not useful for creation of more open structures it does appear to facilitate the organisation step as part of the ADOR process. However, an interesting aspect is the potential to use appropriate organic molecules or/and different conditions for intercalation to shift the IPC-1P layers relative to each other and direct the construction of the alternative, predicted zeolite structures mentioned in the previous chapter.[129]

Calcination of IPC-1P intercalated with organic compounds, such as octylamine, triethylamine, *etc.*, produced in many cases ordered, fully-condensed zeolites IPC-4 (**PCR**) and IPC-2 (**OKO**) as identifiable components (Fig. 13, step 3), as described in Section 5.1. The formation of the IPC-2 (**OKO**) topology requires rationalization as it entails, as described above, the creation of mono-silica bridges between layers leading to S4R units in addition to the process of ordered (commensurate) condensation. The formation of zeolites IPC-4 and IPC-2 during calcinations of intercalated precursors is more favourable when the inter-layer expansion is relatively small (stacking repeat with *d*-spacing less than 21 Å) and decreases with the increasing *d*-spacing.[97,128]

9.2 Swelling of IPC-1P

The other type of IPC-1P intercalation, which involves breaking of the inter-layer hydrogen bonds and swelling, was achieved by applying treatments with cationic surfactants, *i.e.* at high pH. It is usually carried out using a quaternary ammonium surfactant, most often with the hexadecyl tail (*e.g.* C_{16}TMA), in a hydroxide form or as a salt with another organic hydroxide added, like tetrapropylammonium. In this most representative case, the inter-layer distance is expanded by *ca.* 25 Å to overall 35 Å repeat. The influence of the length of the swelling surfactant was investigated with a series of quaternary cations ($C_nH_{2n+1}N(CH_3)_3^+$) with different alkyl chain lengths (n = 8–18). This allowed tailoring of the structural properties of the eventual pillared derivatives, such as the expansion of the inter-layer distance from 16 Å up to 27 Å, and consequently their textural properties.[128]

9.3 Inorganic pillaring of IPC-1P

Swelling and intercalation are rarely the final targets with layered zeolites. They are usually the first step towards additional modifications, especially to generate permanently expanded, delaminated or other more open architectures.

One of the methods of exploiting inter-layer separation achieved by swelling is the introduction of permanent props, which is referred to as pillaring. This is a well-known process applied initially for clays by the intercalation of large inorganic cations based on respective ion exchange characteristics and did not require pre-swelling.[120] Such was not the case for layered metal oxides which had to be swollen first but upon

pillaring with an appropriate silica source, tetraethylorthosilicate, affording mesoporous molecular sieves with a permanently expanded inter-layer distance.[130] The discovered layered zeolites are particularly attractive for such expansion with the eventual goal being catalytic application because of the inherent high activity potential of zeolite frameworks. Framework **MWW** provided the prototype and template for converting layered zeolite precursors into pillared and delaminated structures. The mesoporous character of both pillared and delaminated **MWW** forms[131] is beneficial in many catalytic reactions. They can also be used as supports for other catalysts or active particles utilizing their large external surface.[31,132–141] Pillars may be inorganic, in which case they exhibit thermal resistance to a temperature of 500 °C and higher. Typically, pillars connecting the neighbouring layers are not crystalline and are without a well-ordered distribution (Fig. 13, step 4). Alternatively, pillaring with organic compounds has been carried out to combine advantages of a solid structure of the inorganic part with more easier and broader functionalization potential of organic pillars. These modifications aim to produce materials exhibiting high surface areas with much shorter diffusion paths in comparison to the more condensed structures provided by the standard zeolites.

The successful initial work on swelling and pillaring of IPC-1P[62,92] was significant not only as the source of novel materials but in addition was a validation of the underlying concepts: formation of a precursor (IPC-1P) from a degradable zeolite (**UTL**), its actual layered nature and the ability to be manipulated into various forms. The study of pillaring with TEOS was extended to IPC-1P intercalated/swollen with various organic compounds.[97,128] It resulted in preparation of new mesoporous layered materials with adjustable textural properties. Pillared IPC-1P derivatives have no intra-layer micropores because the layers are dense fragments of the framework (**UTL**, **OKO**, and **PCR**). An adequate inter-layer distance is the essential pre-requisite for achieving pillaring, which appeared not to occur in the case of precursors with relatively small *d*-spacing expansion (less than 5 Å).[97,128] It is probably due to constrained inter-layer space, probably filled with organics preventing an introduction of sufficient amount of silica in between layers. Pillared derivatives of the samples swollen with mixtures of surfactants (C_nTMA) and tetrapropylammonium hydroxide or tetraalkylammonium cations had a broader pore size distribution than those prepared using neat surfactant hydroxide (C_nTMA–OH) solutions. The latter product exhibited pore size distribution in the range of 25–35 Å. The pore size diameter of created mesopores was consistent with the dimensions of the corresponding swelling molecules. Another parameter examined for its effect was the changing ratio of the pillaring agent TEOS, in a chloroform solution, to the swollen precursor (IPC-1SW). As might be expected, too low an amount of TEOS proved insufficient to allow the creation of well-ordered pillared derivatives. On the other hand, an excess of TEOS was also detrimental resulting in inferior textural properties of the final product. Optimal conditions to produce large BET areas and mesopores volumes (up to 900 $m^2\ g^{-1}$ and 0.6 $cm^3\ g^{-1}$, respectively) were found with a TEOS/IPC-1P-swollen ratio = 1.5 (w/w).[128]

9.4 Organic linkers – hybrid materials

The stabilization of swollen zeolite precursors, that is pillaring, has been recently extended to include properly designed organic molecules as props, which produce porous organic–inorganic hybrid materials that can be referred to as organic-pillared materials.[142,143] These covalently bonded organic–inorganic nanosystems combine the usefulness of both components; the advantages of the inorganic part, such as mechanical and structural stability, are complemented by the high flexibility and possibility for functionalization of the organic parts, although the overall thermal stability is decreased due to the presence of organics. Such materials can be useful nonetheless for operation under milder conditions. A noteworthy work in this field reports bridging of **MWW** zeolite layers (MCM-22P) with silsesquioxanes as pillars.[142] It shows the functionalization of benzene rings in the organic part of the hybrid with basic amino groups as resulting in bifunctional acid–base catalysts.

Organic–inorganic hierarchical hybrids with tailored textural properties can be produced from IPC-1P swollen with a cationic surfactant like C_{16}TMA.[143] Bridged silsesquioxanes (BSSs) and polyhedral oligomeric siloxanes (POSs) were introduced into swollen IPC-1SW after two days of stirring at 60 °C. The swelling agent (C_{16}TMA) was then removed by consecutive extraction using NH_4NO_3 and HCl solutions. In the final pillared material the BSSs and POS molecules are covalently bonded to the IPC-1P layers *via* the condensation of terminal alkoxide or silicate groups with terminal Si–OH groups of IPC-1P. Thus, they create pillared materials, where organic or well defined inorganic inter-layer props could be recognized (based on XRD, TEM, thermogravimetry and micropore size distribution analysis). The BSSs molecules used for modifications were 1,4-bis-(triethoxysilyl)benzene (BSS1), 1,2-bis-(triethoxysilyl)ethane (BSS2) and 4,4-bis-(triethoxysilyl)-1,1′-biphenyl (BSS3) (Fig. 13, step 5). Inorganic props were introduced using octakis(tetramethylammonium)-T8-siloxane.[143] The inter-layer space contains more than one linker molecule connecting the layers. This creates mesoporous or hierarchical micro-mesoporous systems exhibiting BET areas higher than 1000 $m^2\ g^{-1}$, micropore volumes above 0.3 $cm^3\ g^{-1}$ and a total pore volume over 1 $cm^3\ g^{-1}$. Thermal stability of these hybrid materials is relatively high (up to 350 °C). Textural properties of this type of layered materials with organic pillars can be adjusted by varying the ratio of the layered material used *versus* the amount of organic species forming pillars.[143]

10. Key parameters of ADOR application

The previous sections have described the mechanism of the ADOR process and the methods by which new materials have been prepared, concentrating on the work that has been done on the **UTL** system. An important feature of any synthetic

development is an illustration of the requirements and limitations of the process, and by understanding these features one can then look to generalise the processes and apply the concepts to other systems. With this goal in mind we will now discuss the key parameters of the ADOR mechanism and its potential applicability to other germanosilicates.

10.1 Germanosilicate zeolites

In the last decades, germanium has been found to preferentially occupy double-four-ring units (D4R).[78–80,144] A series of germanate materials with D4Rs have been reported, for instance zeotypes ASU-7 (**ASV**)[145] and IM-10 (**UOZ**),[146] both consisting mostly of D4R units with 3-dimensional framework connectivity. The preferential location of Ge in D4Rs is attributed to less strained Ge–O–Ge angles (154 ± 9°) in comparison to Si–O–Si angles (130°) and the stabilizing effect of germanium during D4R formation.[147] This effect was demonstrated with ITQ-7 which can be prepared as a pure silica material as well as germanosilicate.[144] The effect of replacing Ge for Si was also investigated by density functional theory.[148] The enthalpies established for the formation of Ge-containing zeolites (*ca.* 15–20 kJ mol^{-1}) are higher than those for pure-silica zeolites (7–14 kJ mol^{-1}), both related to quartz formation. Nevertheless, this kind of instability does not necessary mean a disadvantage and can be used for selective transformation as the present example of **UTL** clearly demonstrates.

The benefits of using germanium, which promotes the formation of D4R units, sometimes together with a fluoride medium (F^- also stabilizes D4Rs) has been manifested in the synthesis of numerous novel zeolite structures.[43,71,72,78,81,146,149–165] It can be traced to the first synthesis of the all-Ge zeolite polymorph BEC[149] and subsequent enormous expansion at the beginning of 2000s.[151] It is illustrated in Table 3 where zeolites prepared as germanosilicates and containing D4R or double-three-ring (D3R) units are summarized. Nevertheless, the small D4R unit is a part of the framework not just in microporous germanosilicates but also in aluminosilicates, *e.g.* zeolite A (**LTA**),[166] ITQ-27 (**IWV**),[167] UZM-5 (**UFY**),[168] in borosilicate ITQ-52 (**IFW**),[169] in purely siliceous zeolites, *e.g.* ITQ-50 (**IFY**),[170] IM-17 (**UOV**),[171] in AlPO or CoAlPO type of materials, *e.g.* AlPO-16 (**AST**),[172] CoAPO-50 (**AFY**),[173] or in mesoporous germanosilicate ITQ-37 (–**ITV**).[156] Some zeolites containing D4R units were synthesized first as (alumino)silicate zeolites and later with germanium incorporated, for instance ITQ-29 (**LTA** type)[174] or ITQ-7 (**ISV** type).[144]

A theoretical study of many germanosilicates and subsequent experimental results indicate what may be the key factors for successful top-down synthesis of 2D layers and for the ADOR application. It includes the following: (1) the presence of germanium in a framework; (2) the specific location of germanium in D4R/D3R units; (3) the location and connectivity of D4R/D3R units inside a framework; (4) the dimensionality of the channel system present in a parent zeolite; (5) the presence of other hydrolytically sensitive elements in the framework; and (6) crystal size of a parent zeolite. These parameters are discussed in the following text.

10.2 Content of germanium and its location

Although germanium preferentially occupies D4R/D3R units, in some zeolites, with high germanium content it can also

Table 3 The list of germanosilicates containing D4R/D3R units. Adopted from the IZA website[70]

IZA code	Type material	Channel dimensionality	Channels	Type of double-ring unit	Location of double-ring in	First reported (patent/paper)
BEC	FOS-5 beta polymorph C	3-Dimensional	12-12*R*	D4R	3D	2000[149]
IRN	ITQ-49	1-Dimensional	8*R*	D4R	2D	2012[162]
IRR	ITQ-44	3-Dimensional	18-12*R*	D3R, D4R	3D	2010[150]
–IRY	ITQ-40	3-Dimensional	16-15*R*	D3R, D4R	3D	2010[164]
ISV	ITQ-7	3-Dimensional	12-12*R*	D4R	2D	2002[144] [a]
ITG	ITQ-38	3-Dimensional	12-10-10-10*R*	D4R	1D	2012[180]
ITH	ITQ-13	3-Dimensional	10-10-9*R*	D4R	1D	2002[153]
ITR	ITQ-34	3-Dimensional	10-10-9*R*	D4R	1D	2008[154]
ITT	ITQ-33	3-Dimensional	18-10*R*	D4R	2D	2006[181]
–ITV	ITQ-37	3-Dimensional	Mesoporous	D4R	3D	2009[156]
IWR	ITQ-24	3-Dimensional	12-10-10*R*	D4R	1D	2003[165]
IWS	ITQ-26	3-Dimensional	12-12*R*	D4R	3D	2008[157]
IWW	ITQ-22	3-Dimensional	12-10-8*R*	D4R	1D	2003[81]
LTA	ITQ-29	3-Dimensional	8*R*	D4R	3D	2004[174] [b]
POS	PUK-16	3-Dimensional	12-11*R*	D4R	2D	2014[163]
SOF	SU-15	3-Dimensional	12-10*R*	D4R	3D	2008[158]
STW	SU-32	3-Dimensional	10-8*R*	D4R	3D	2008[158]
SVV	SSZ-77	0-Dimensional	6*R*	D4R	1D	2008[159]
UOS	IM-16	3-Dimensional	10-8-8*R*	D4R	1D	2007[171]
UOZ	IM-10	0-Dimensional	6*R*	D4R	3D	2004[146]
UTL	ITQ-15/IM-12	2-Dimensional	14-12*R*	D4R	1D	2004[71,72]
UWY	IM-20	3-Dimensional	12-10-10-10-10*R*	D4R	2D	2010[161]
	ITQ-21	3-Dimensional	12*R*	D4R	3D	2002[78]
	ITQ-43	3-Dimensional	28-12-12-12*R*	D4R	2D	2011[182]

[a] **ISV** was first reported in 1999 as pure silica zeolites, later in 2002 prepared as germanosilicates. [b] **LTA** was first reported in 1956 as aluminosilicates, later in 2004 prepared as aluminogermanosilicates.

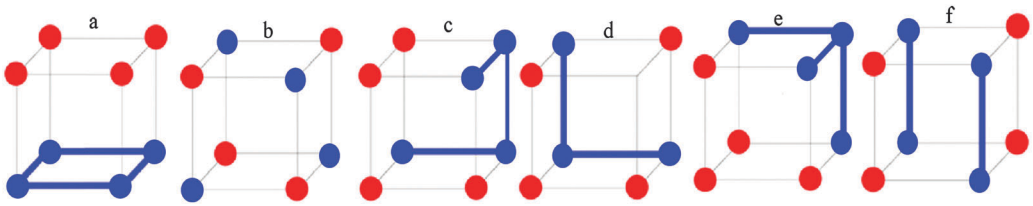

Fig. 14 Different localizations of Ge atoms (red) in [4Si,4Ge] D4R units. Si–O–Si linkages supposed to remain intact under acidic conditions are presented in blue.

occupy other T-positions. Due to hydrolytical instability of the Ge–O(T) bonds it would mean that acid hydrolysis cannot be selective in terms of breaking of T–O bonds in germanium D4R units. Thus, for the purpose of top-down synthesis, *i.e.* 3D–2D transformation, the suitable candidates are germanosilicates with most of germanium atoms located preferentially in D4R/D3R units and with minimum occupancy in the layers. This can be influenced by experimental conditions, particularly by an amount of germanium in a reaction gel, appropriate SDA *etc.* Considering that all Ge atoms are only in D4R units one can assume that for the full removal of D4Rs from the framework, minimally four Ge atoms should be the part of each D4R unit. Our experiments have shown that some silicon is also transferred into solution during the hydrolysis step, which explains why the entire D4R unit is removed from UTL. However, it was demonstrated by Tuel *et al.*[83] that a sufficiently high amount of Ge atoms (in this case >4 Ge/D4R) alone is not always enough to break all connections between the layers. In general, six various distributions/configurations of Ge atoms within a D4R unit are possible, see Fig. 14. Only in the cases (a) and (b) we can suppose a full separation of the layers. In other formations there exist Si–O–Si interlayer bonds which are supposed to be stable under acid conditions. Thereby, the acid solution treatment may only extract Ge atoms while preserving the framework with the layer connectivity. The layers would only then be disconnected if the resulting Q^1 and Q^2 species produced are also unstable towards hydrolysis under these conditions. Hence, for full layer separation it is preferable that more than 4 Ge atoms present in each D4R unit and in addition, it is likely that different arrangements of the Ge will have an important effect. The ideal example is given by zeolite **UTL** where the Si/Ge ratio 4.3 indicates the presence of, on average, 7 Ge atoms per D4R (Fig. 1). In the case of the Si/Ge ratio 6 there are still 5 Ge atoms in the D4Rs. Tuel *et al.* studied the location of Ge atoms in the D4R unit using ^{19}F MAS NMR and ^{1}H–^{29}Si CP/MAS NMR.[83] They consider the germanium occupying only D4R units and that there are 4 Ge atoms per D4R unit. Based on their results, in **UTL** germanium preferentially forms one germanate four-ring attached to the layer and thus the layers can be fully disassembled. In the case of other germanosilicates like **IWW** or **ITH** according to Tuel, germanium distribution is more even at all T-sites in D4R.[83]

10.3 D4R/D3R units in the framework

Clearly the key feature of germanosilicates that can be used for the ADOR process is the presence of D4R/D3R units. Table 3 shows 24 germanosilicates containing D4R units. Zeolites **IRR** and **–IRY** contain, besides D4Rs also D3R units in their frameworks. Germanosilicates with only D3R units and not D4R units have not been discovered yet.[151] We can look at the D4R units considering their location in the framework like 1-dimensional, *i.e.* they appear only along one axis and create a sort of supportive pillars between the layers. This is the case of zeolites **UTL**, **ITH**, **IWW**, and five other germanosilicates (see Table 3). Breaking of all inter-layer bonds *via* hydrolysis of D4R units should lead to 2-dimensional lamellas like IPC-1P in the case of **UTL** zeolites. Six germanosilicates, for instance **IRN** and **UWY**, have D4Rs in two directions, which we designate as a 2-dimensional location. It means they are located between the layers as well as they are part of the layers along one dimension. Hypothetically, acid hydrolysis of germanium-rich D4R units would cause the separation of the framework along two "cleavage lines". It may result in 1-dimensional zeolitic fibres or chains. Generally, after hydrolysis there is a dense grid of silanol groups as residues after hydrolysed D4Rs. Terminal Si–OH groups can be hydrogen bonded with other silanols from neighboring chains.[95] Therefore, zeolitic chains might be ordered or partially ordered with respect to each other *via* hydrogen bonding. The last group is germanosilicates with 3-dimensional distribution of D4Rs, *i.e.* D4Rs are part of the framework along all the three directions. There are ten zeolites with this D4R-distribution, for instance **BEC**, **IWS**, **IRR** or **STW** (see Table 3). Considering that all D4R/D3Rs are Ge-rich enough to be fully hydrolysed, the acid treatment would lead to almost full fragmentation of the framework as it would take place along all the three directions. At the first instance, it might be seen as of little use and undesirable for destroying the framework, which was laboriously synthesized in the first place. Nonetheless, it may actually result in fractions or islands of a zeolitic framework. In other words, we may prepare small zeolitic units. The challenge is whether there is potential for using them as building blocks, organising in some way or even utilizing them in the synthesis as starting nuclei. Moreover, there are obvious problems connected with the characterization of such small units and thus finding a suitable characterization technique can be quite challenging.

10.4 Channel system of parent zeolites

Until now we discussed the parameters impacting the efficiency of D4R hydrolysis. The next parameter to be assessed is the stability of potential dense layers. The channel dimensionality has turned out to be a very important feature regarding the layer stability. Table 3 shows there is only one germanosilicate

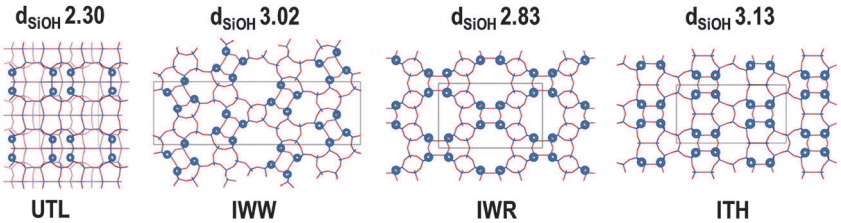

Fig. 15 2D layers of **UTL**, **IWW**, **IWR** and **ITH** with highlighted surface silanol groups (blue circles) and unit cells (in grey). The silanol density, d_{SiOH}, is calculated for surface 1 nm^{-2} (for more details see Table 2).

with a 1-dimensional channel system, zeolite **IRN**, and one germanosilicate with 2-dimensional channel system **UTL**. In this respect, zeolite **UTL** is a special case in the group of germanosilicates as the location of its D4Rs is only 1-dimensional, *i.e.* just between the adjacent layers, and thus it is an ideal precursor for top-down synthesis of a lamellar zeolite. Nevertheless, there are two more exceptions, **SVV** and **UOZ**, which are considered to have no channel system having only 6-ring cages. All other germanosilicates have 3-dimensional channel systems. In the case of **UTL** zeolites, the disassembly leads to layers with no intra-layer porosity as the channel system (14-12-ring) is selectively destroyed by removing the D4R units. As a result, IPC-1P layers are dense silicate nanosheets. For easier comparison we consider now only germanosilicates as if having only 1-dimensional location of D4Rs, *i.e.* D4Rs only between layers. If all inter-layer bonds are hydrolysed, such layers would still possess intra-layer zeolite-like channels going perpendicular through them. For instance **IWW**-layers would have 12-8-ring channels, **IWR**-layers 12-ring channels, **ITH**-layers 9-ring channels, *etc.* Framework densities of the appropriate layers were calculated based on the DFT level of theory.[110] The **UTL**-layer has the highest T-atom density in comparison to **IWW**, **IWR**, or **ITH** (84.6 *vs.* 71.0, 68.7, 76.4 T-atoms in 10^{-3} $Å^{-2}$, respectively).[110] Moreover, 2D layers obtained from these germanosilicates also differ significantly in the surface silanol density, see Table 2 and Fig. 15. It should be kept in mind that a higher density of silanol groups on a surface leads to the formation of a higher concentration of hydrogen bonds between neighboring layers. Therefore, the inter-layer non-covalent bonds can quite strongly restrict breaking them to enable inter-layer intercalation.

10.5 Heterosubstituted germanosilicates

The presence of other heteroelements in addition to germanium may introduce other centers of instability into the framework, especially if they are sited near the D4R/D3R units. Particularly under severe conditions of hydrolysis (up to 12 M HCl at high temperature) we can expect removal of incorporated elements into extra-framework positions in part or totally from the framework (mainly in the case of boron, aluminium or iron).[175,176] For instance, in the case of boron ZSM-11 it was proven that even a mild chemical treatment in 0.1 M HCl leads to the formation of extra framework B^{3+} species.[175] Only some germanosilicates have been so far prepared exclusively in the presence of other element, *e.g.* **IWR** with boron[177] or aluminium[165] or **IRR** with aluminium.[150] The presence of other hydrolytically sensitive heterolement can decrease the selectivity in disassembling the layers and/or can increase the number of framework defects or extra framework species.[178,179]

10.6 The effect of crystal size

It is clear from the discussion of the ADOR mechanism that kinetics plays an important part in determining the outcome of the process. There is a question whether or how the crystal size may influence the hydrolysis process, particularly under conditions where only a certain part of layers undergo de-intercalation and part reorganisation (*e.g.* the synthesis of IPC-6). Zeolite **UTL** crystallizes as quite uniform rectangular crystals of sizes in the range 10–60 μm but with a very thin third dimension.[92,93] Sometimes, even bending of such thin plate sheets without breaking can be observed. The layers are stacked along the *a* axis, which is the shortest dimension of the crystal. The thickness of the crystals is in the 0.01–0.1 μm range, moreover, in some cases, regions of only one or two unit cell thickness were found.[92] The thickness of the **UTL** monolayer (corresponding to average step high of the terraces) was determined by AFM to be about 14 Å, which corresponds to half the unit cell, 29 Å, as well as the value for d_{200}-spacing found by XRD, 14.4 Å.[93] Taking the maximum thickness of the **UTL** crystal, about 0.1 μm, the number of monolayers stacked on top of each other should be around 70. It was proposed that the hydrolysis, which removes D4R units from the layers, is initiated at the edges of the crystals and then causes the unzipping effect throughout the whole crystal. In comparison to **UTL**, the other germanosilicates like **ITR**, **IWW** or **IWR** form small crystals of size less than 6 μm and usually crystallize in agglomerates.[177] None is similar in morphology with **UTL**. The crystals are supposed to consist of more than 70 layers as they are not as thin as **UTL** sheets. Hence, there is a question about the stability of such small crystals under harsh hydrolysis conditions (up to 12 M HCl at high temperature) and the effectiveness of the hydrolysis deeply in the crystal. As it was discussed in previous sections, highly acidic environments enhance making and breaking of silica bonds, which enables the reorganisation of atoms from intra-layer T-sites into inter-layer space forming new bridges. With large sheets of **UTL** monolayers, the acidic conditions do not markedly influence the stability and morphology of crystals.[93] However, the impact of highly acidic solution on small crystals with a large number of ordered layers has not been thoroughly studied and thus it remains debatable.

Based on the analysis of all aforementioned parameters and their relationship with the full hydrolysis feasibility, zeolite stability and potential for layer manipulation, we suggest that ideal candidates for the ADOR method are germanosilicates having enough germanium located mostly in D4R/D3R units (at least 6Ge/D4R), which are located only between the zeolite layers, with the so called D4R 1-dimensional location. The stability advantage of potential 2D zeolites without channels through layers was discussed as well as the impact of a high concentration of surface silanols bonds on the layer manipulation. Nevertheless, we believe that choosing appropriate experimental conditions can overcome/suppress some undesired effects connected with the individual zeolite frameworks. Thereby, from 24 germanosilicates listed in Table 3 at least 8 zeolites seem to be the most suitable candidates for top-down synthesis of 2D zeolites: **ITG**, **ITH**, **ITR**, **IWR**, **IWW**, **SVV**, **UOS**, and **UTL**. There is one more promising candidate not mentioned in Table 3, zeolite **IWV**. It has not been included as it has been so far prepared only as aluminosilicate. It contains D4R units in the framework has a 2-dimensional channel system and D4Rs only between the layers – all aspects similar to zeolite **UTL**. The combination of all factors based on the aforementioned discussions makes **IWV** a very promising candidate for the ADOR application. Notwithstanding, the incorporation of germanium into D4Rs is essential and without it the ADOR can be hardly efficient, until we find methods for selective breaking of other types of bonds or to build in weaknesses where they did not exist before, preferably by design.

The essential germanium presence for successful ADOR represents the main drawback of this methodology due to the high cost of germanium. Nevertheless, this can be eliminated by Ge recycling. Most of it is lost during the disassembly step. After filtering the solid product the solution contains both germanium and siliceous species in various ratios depending on the acidity of the hydrolysing environment. Therefore, the separation of siliceous and germanium species is one of the requirements for successful reuse of germanium in the synthesis of the parent zeolite.

11. ADOR application to other zeolites

11.1 The theoretical approach

The concept of ADOR demonstrated for **UTL** transformation into IPC-2, IPC-4, IPC-6 and IPC-7 zeolites[63] can be extended in a number of directions: (i) calcination of a 2D layered material without or upon a regular shift of adjacent layers (a modification of an organisation step) has been discussed above for **UTL** and several hypothetical zeolite topologies were proposed (for more see Section 8). (ii) Various inter-layer pillars can be considered and even a regular alternation of different pillars is of interest. (iii) In addition to **UTL** the ADOR protocol can be applied to other existing zeolite structures; of particular interests are those containing D4R pillars separating zeolite layers, such as zeolites **IWW**, **IWV**, **IWR**, **ITH**, and **ITR**. The framework parameters influencing the suitability of individual zeolites for the ADOR method were discussed in detail in the previous chapter. Note that in at least *in silico* investigation (using molecular modeling techniques) all these ADOR extensions can be exploited, including any of the combinations of the above-mentioned extensions. Clearly, the ADOR strategy offers a variety of modifications that could lead to the synthesis of new zeolites that cannot be obtained by a traditional solvothermal route. While finding suitable reaction conditions for the synthesis of new zeolites *via* an ADOR protocol represents a great challenge for experimental chemists. It is relatively easy to follow the ADOR protocol *in silico*. The structure and properties of 3D zeolites that could be obtained by the ADOR process or its extensions were recently investigated computationally.[108,110]

Compared to previous theoretical investigations leading to millions of hypothetical zeolite structures[116,117] the computational investigation following the ADOR protocol led to only few new zeolite structures. However, the probability that some of the zeolites proposed in such a way is synthesized in near future is significantly larger than for any of the previously proposed hypothetical zeolites. In fact, none of the computationally proposed zeotypes have been synthesized in the aluminosilicate form (only the VIP-5 aluminophosphate synthesized in 1988[183] had the predicted **VFI** structure type[184]) except for polymorph C of Beta zeolite (**BEC**),[185] which had been earlier predicted by Newsam *et al.*[186] based on the shift of dense zeolite layers, a somewhat similar concept of layer manipulation as adopted herein. Zeolite frameworks **EMT** and the unapproved yet MCM-71 were anticipated by Breck.[187]

The ADOR protocol has been followed computationally for **UTL**, **IWV**, **IWW**, **IWR**, **ITH**, and **ITR** zeolites, considering the –D4R zeolites[108] and –S4R zeolites.[110] Following the strategy described in Section 8, layer manipulation a total of 22 topologically unique zeolite structures was obtained upon direct condensation of 2D zeolite layers (–D4R zeolites). Significantly a larger number of unique zeolite structures were achieved when connecting 2D zeolite layers *via* S4R pillars (Fig. 12) and only 27 zeolites with the lowest energy with Sanders–Leslie–Catlow (SLC) potential[188,189] were re-optimised at the DFT level. The topology of new zeolites with the number of unique T atoms not exceeding eight were confronted with existing database of zeolite structures and some of them were found in the atlas of prospective zeolite structures[190] (for details see ref. 108). All predicted zeolites were characterized by the feasibility factor, LID criteria, and their energy/density plots were reported. The LID criteria reported in ref. 110 are satisfied for structures with framework energy FE_{DFT} equal to or lower than that of corresponding parent zeolites. The only exception is the **ITH**-S4R group of zeolite, for which the LID criteria are satisfied even if FE_{DFT} is higher (up to 2 kJ mol^{-1} TO_2^{-1}) than the corresponding value for parent **ITH** zeolites. Feasibility of zeolite synthesis was discussed based on the framework energy (FE_{SLC}) and framework density (FD_{SLC}); two distinct situations were found for investigated materials: (i) for zeolites derived from **UTL**, **IWV**, and **IWW** parent materials there is always one energetically preferred structure (one without a lateral shift) in –S4R and one in –D4R families while other structures are energetically higher (see Fig. 16).

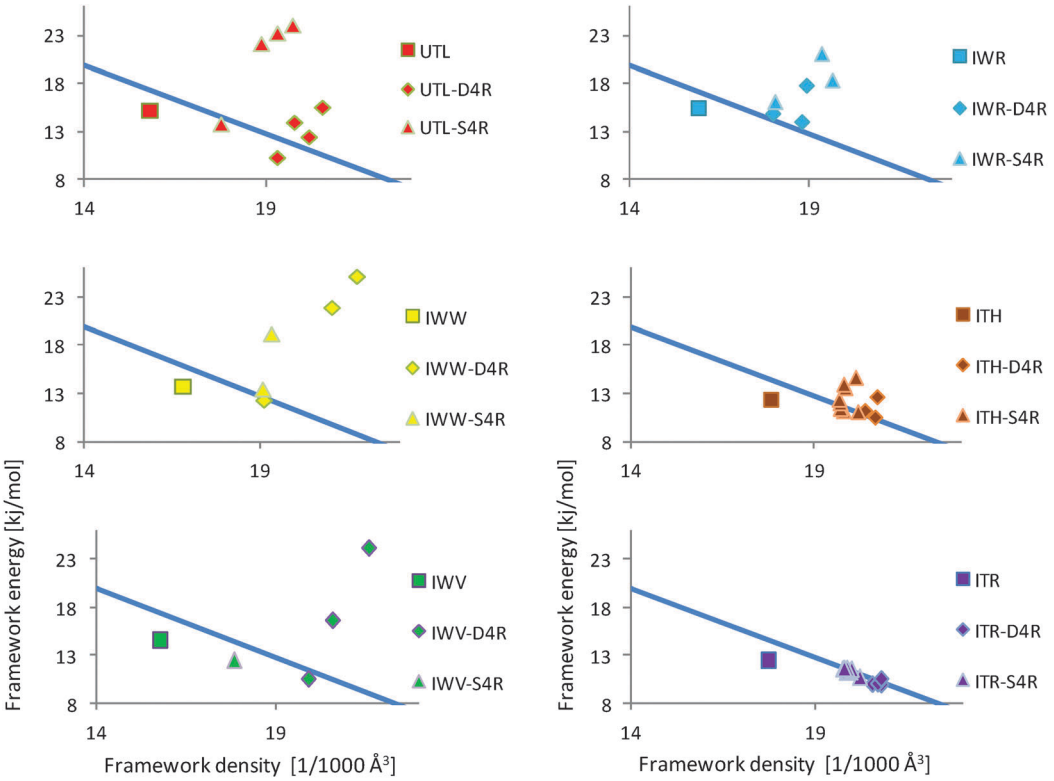

Fig. 16 Framework energy *vs.* framework density plots calculated at the FF level[96] for new zeolites obtained computationally following the ADOR protocol. The energy/density plot for existing zeolites is depicted as a blue line; parent zeolite and zeolites obtained in –D4R and –S4R families are shown as squares, diamonds, and triangles, respectively.

In the case of **UTL** and **IWV** zeolites the energetic preference of one structure can be understood in terms of a lower concentration of surface silanol groups (Table 2) that results in a larger lamellar deformation required for the layer connectivity with the inter-layer shift. In the case of **IWW** zeolites with a large density of surface silanol groups in corresponding 2D layers the energy differences are due to the orientation of surface silanol quadruplets. (ii) More than one energetically preferred structure was found for zeolites derived from **IWR**, **ITH**, and **ITR** parents (Fig. 16). This is due to the large concentration of surface silanol groups allowing various layer connections without a significant framework deformation.

The structure and feasibility characteristics were also calculated for zeolites obtained from IPC-1P layers connected with regularly alternating inter-layer pillars, considering a direct layer connection (oxygen atom linkers), the connection *via* S4R linkers, and the connection *via* D4R linkers. No inter-layer shifts were considered. All resulting materials were found to have lower FE_{DFT} than the parent **UTL** material and they all satisfied the LID criteria.[110]

11.2 The experimental results

Successful transformation of the 3D germanosilicate **UTL** zeolites into the 2D IPC-1P material[62] opened up new pathways for the manipulation of the IPC-1P units to produce new ADORable zeolites like IPC-2,[63] IPC-4,[63] IPC-6[91] and IPC-7[91] differing in the connectivity of the layers while having the same topology of the layers. This inspired the investigation of extension of the ADOR strategy to other zeolites comprising Ge-enriched D4R units connecting individual silica layers. The role of the zeolite topology and chemical composition of parent germanosilicates in the hydrolysis step – the disassembly is now discussed. Ge distribution in the framework of zeolites and its role in the disassembly process will be discussed in detail.

Recently, the ability of Ge to: (1) induce the formation of small D3R and D4R SBUs in the early stages of the crystallization process;[191] (2) accelerate the crystallization of zeolites, containing D4Rs[77,192] and (3) stabilize such structures[193,194] was exploited to synthesize a number of previously unknown germanosilicate zeolites.[43,72,156,164,195–197] In 2003, Corma and coworkers synthesized 3 new germanosilicate zeolites **ITH**,[82] **IWW**[81] and **IWR**[165] (Table 4) in highly concentrated reaction media ($H_2O/T^{IV} < 10$, where T is the zeolite framework tetrahedral atom, Si or Ge) using hexamethonium dihydroxide as the structure-directing agent. While **IWW** and **ITH** crystallized from pure germanosilicate medium, **IWR** zeolites having the highest void volume among competing phases can be only prepared in the presence of boron or aluminum ions compensating a positive charge of the occluded SDA.[193] At the same time, F^- anions acted cooperatively with Ge in the stabilization of not only D4R units but also small $[4^15^26^2]$ cages present in the **ITH** structure.[198] Later on, polymorph B of **ITH** zeolites (named **ITR**) possessing the same topology of 2D layers as **ITH** (Fig. 17) was synthesized using propane-1,3-bis(trimethylphosphonium)

Table 4 Structural characteristics of some germanosilicates as precursors for ADOR application

Zeolite	Pore size	Unit cell composition	D4R per u.c.	Si/Ge corresponding to 50% Ge population in D4Rs
ITR	9-ring 4.1 × 5.1 Å 10-ring 4.7 × 5.8 Å 10-ring 4.8 × 6.0 Å	$T_{112}O_{224}$	6	3.7
ITH	9-ring 4.0 × 4.8 Å 10-ring 4.8 × 5.1 Å 10-ring 4.8 × 5.3 Å	$T_{56}O_{112}$	2	6
IWW	8-ring 3.3 × 4.6 Å 10-ring 4.9 × 4.9 Å 12-ring 6.0 × 6.7 Å	$T_{112}O_{224}$	4	6
IWR	10-ring 4.6 × 5.3 Å 12-ring 5.8 × 6.8 Å	$T_{112}O_{224}$	4	6
UTL	12-ring 5.5 × 8.5 Å 14-ring 7.1 × 9.5 Å	$T_{76}O_{152}$	2	8.5

hydroxide as the SDA.[198] In contrast to **ITH** zeolites (polymorph A) with sheets extending in the *bc* plane and stacking along the *a* direction in the AAA sequence, the **ITR** stacking sequence is ABAB, where B corresponds to the A sheet of **ITH** after applying a 180° rotation around the *b* axis and a translation of 1/2 along the *c* axis.[198] Similarly to **UTL**, the topologies of these materials can be viewed as dense two-dimensional (2D) layers separated by D4R bridging units (Fig. 17). XRD refinement[72] and ^{19}F NMR[83] revealed the exceptional location of Ge atoms in-between the layers of **UTL** zeolites, which created the background for a selective cleavage of the inter-layer bonds in acidic medium at preservation of the layers, *i.e.* successful passing of the disassembly step. At the same time, the preferential location of Ge (*ca.* 90% of Ge) in D4Rs in-between silica layers of **ITH**,[82] **ITR**,[198] **IWW**,[199] **IWR**[200] zeolites makes them good candidates for applying the ADOR strategy. However, the occupation of up to 10% of the intra-layer T-sites by Ge atoms[82,198–200] may influence the hydrolytic stability of crystalline layers with possible negative consequences as discussed in the previous chapter.

Structural transformations of **ITH**, **ITR**, **IWR**, and **IWW** zeolites in acidic medium were extensively investigated in many studies.[83,177,201–203] The influence of treatment conditions (*e.g.* concentration of acid used, time, temperature *etc.*) and chemical composition of the parent zeolite on the hydrolysis result was carefully addressed. The most important results for individual zeolites as well as general trends for germanosilicates under study can be summarized as follows.

The Si/Ge ratio in parent zeolites impacts the number of labile Ge–O(T) inter-layer bonds and consequently influences the hydrolytic stability of respective germanosilicates. Assuming that most of Ge atoms are located in D4Rs[204] and at least 50% of T-atoms in D4Rs should be occupied by Ge for successful hydrolysis, the roughly estimated Si/Ge ratio appropriate for the full disassembly of **ITH** zeolites is lower than 6 (Table 4). When hexamethonium dihydroxide is employed as the structure directing agent for the synthesis of **ITH** zeolites, samples with high Ge concentrations (Si/Ge ratio <7) were not yet achieved.[82,192,193] Indeed, a big fraction of pure silica D4R units was detected in hydrolytically stable **ITH** zeolites having a Si/Ge ratio >7 by means of ^{19}F NMR spectroscopy.[177] Fortunately, high Ge-containing **ITH** zeolites can be prepared using *N*,*N*,*N*′,*N*′-tetramethyl-1,6-hexanediamine (TMHDA) as the SDA.[205] However, even **ITH** zeolites characterized by Si/Ge = 4.4, which is higher than the estimated ratio of Ge occupying half of the D4R, was shown to possess some fraction of [7Si, 1Ge] D4R, preventing a full disassembly of the zeolite in acidic medium.[177] Alternatively, Tuel *et al.* considered the unconventional distribution of Ge atoms in D4Rs (Fig. 14c–f) providing a number of hydrolytically stable Si–O(Si) inter-layer linkages as a reason of **ITH** zeolite (Si/Ge = 4.5) resistance in acidic medium.[83] When the Si/Ge ratio in **ITH** zeolites further decreases to 2.5 only D4R units with 50% Ge occupation were detected by ^{19}F MAS NMR. The acidic treatment (0.01 M HCl, 24 h) of the respective Ge-rich

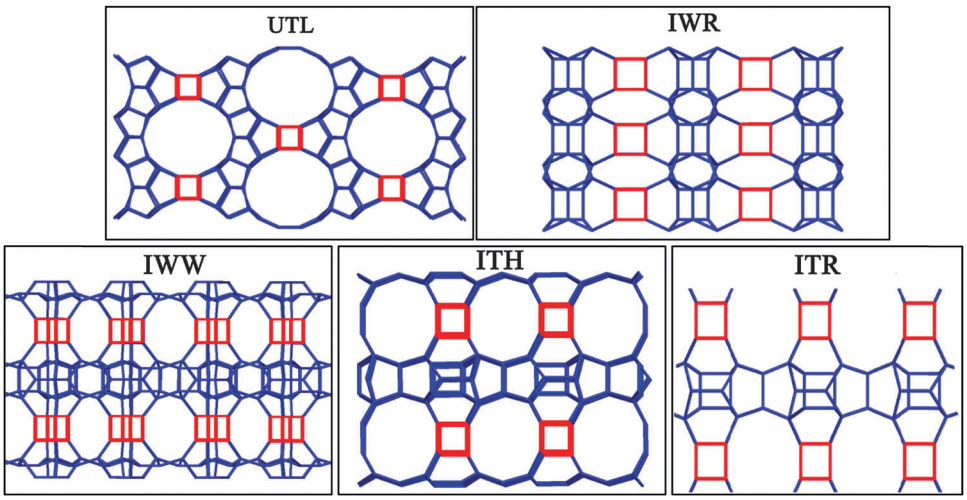

Fig. 17 The structure of zeolite **UTL** (001 projection), **IWR** (100 projection), **IWW** (010 projection), **ITH** (010 projection) and **ITR** (100 projection).

ITH sample resulted in the formation of a 2D layered solid.[177] One can assume that some favourable Ge locations in D4R SBUs (*e.g.* shown in Fig. 14a and b), likely governed by TMHDA, led to successful delamination of **ITH** (Si/Ge = 2.5). The obtained layered material showed intra-layer diffraction lines characteristic of **ITH** topology while characterized by shorter inter-layer distances (decreased by *ca.* 2.6 Å) and lower Ge content (Si/Ge = 100).

Similarly, the disassembly of germanosilicate **ITR** (Si/Ge = 2.4) zeolites having about 50% of Ge in D4R units was achieved by selective hydrolysis in 0.01 M HCl for 24 h.[177] The obtained layered derivative was characterized by a decreased inter-layer distance (difference is *ca.* 1.70 Å, Fig. 18) resulting from further contraction of interlayer space upon calcination. With decreasing Ge content the hydrolytic stability of **ITR** (Si/Ge = 4.6) increased resulting in a smaller shrinkage of the inter-layer distance (*ca.* 0.85 Å, Fig. 18). It evidences the preservation of some inter-layer connections even when the removal of most Ge atoms from the framework took place (Si/Ge = 30 *vs.* 4.6).

Complementary results were obtained in ref. 203 comparing the hydrolytic stability of Ge-rich (Si/Ge = 3.1–3.6) and Ge-poor (Si/Ge = 6.4) **IWW** zeolites. According to Rietveld refinement of the synchrotron data, the only sites with significant Ge occupancy were present in D4R units. The D4R in Ge-rich **IWW** (Si/Ge 3.6) has statistically 6 Ge atoms and 2 Si atoms, [6Ge, 2Si], *i.e.* one purely Ge-four-ring and second occupied by half Si atoms. In contrast, the average site occupancy in Ge-poor **IWW** (Si/Ge 6.4) was found to be near the even-balanced distribution [4Ge, 4Si], however, it does not form one pure Ge-four-ring and second pure Si-four-ring but it has a more random distribution of Ge atoms over all T-sites in D4R. Thus, Ge-rich **IWW** can be expected to be more easily disassembled into a layered material than Ge-poor **IWW**. Ge-rich **IWW** (Si/Ge 3.1) was treated with acidic solutions (0.1 M–12 M HCl) at ambient temperature leading to a layered material called IPC-5P with the inter-layer distance reduced by 1 to 3 Å depending on the applied conditions. Similar to other germanosilicates discussed in this chapter, the ambient temperature turned out to be more efficient in the disassembly of the structure with layer preservation. Using higher temperature (85–100 °C) led to more damage of the structure. It is probably connected with the fact that all these germanosilicates have 3-dimensional channel systems having channels through the layers as it was discussed in the previous chapter. In the case of **IWW** layers possess two types of channels, 12- and 8-ring running across them, which makes them less stable in comparison with IPC-1P layers formed from zeolite **UTL**. After a series of treatment when IPC-5P reacted with diethoxydimethylsilane the structure of **IWW** was restored as an almost pure siliceous framework (Si/Ge 73). On the other hand, the same acidic conditions applied to Ge-poor **IWW** (Si/Ge 6.4) led only to extraction of Ge atoms with the preservation of the original framework. The generated structural defects can be filled with aluminum atoms resulting in restored **IWW** zeolites with a Si/Ge ratio of 115 and a Si/Al ratio of 27 (ref. 203).

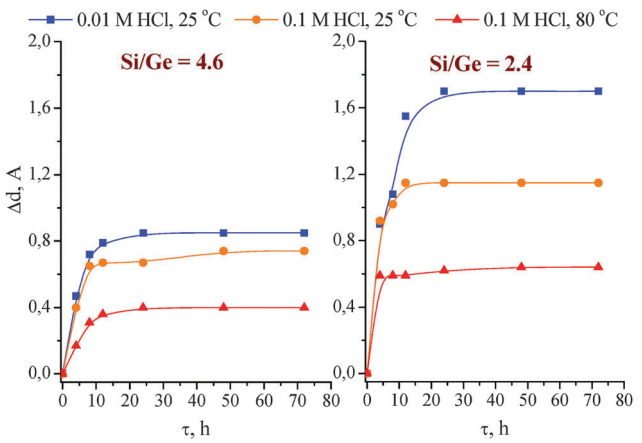

Fig. 18 Decrease in the inter-layer *d*-spacing for the hydrolyzed derivatives of **ITR** zeolites as a function of time.

While the full hydrolysis of inter-layer Ge–O(Si) bonds in the medium-pore **ITH**, and **ITR** zeolites is achieved within 24 h, in the case of large-pore **IWR** (Si/Ge = 6.9, 14.8 mol% B) a substantial shift of the inter-layer 001 diffraction line (the shortening of the inter-layer distance by *ca.* 1.93 Å) with preservation of intra-layer 110 and 200 reflections took place after 5 min of the treatment with 0.01 M HCl.[177] Similar results were achieved within 5 min of the treatment of extra-large pore **UTL** zeolites (Si/Ge = 4.5) with 0.1 M HCl.[92] Thus, one can infer that the optimal duration of acid treatments is determined by diffusion of ions into and out of the micropore system of germanosilicate zeolites. In other words, the larger pores accelerate the diffusion[206] and therefore, a shorter time is required for successful hydrolysis. Further prolonged acid treatment of borogermanosilicate **IWR** caused structural changes in its zeolitic layers, which are likely connected with the hydrolysis of intra-layer B–O bonds. Thus, the random distribution of B atoms representing additional centers of hydrolytic instability in the layers limits the applicability of selective disassembly approach to borogermanosilicate zeolites confirming the general expectation discussed in the previous chapter. Indeed, **IWR** (Si/Ge = 6.9, 14.8 mol% B) zeolites lost most of Ge (Si/Ge = 31) and all boron when subjected to acidic hydrolysis.[177]

The general phenomena observed during the hydrolysis of germanosilicates **ITH**, **ITR**, and **IWW** can be summarized as following: (i) the decreasing inter-layer distance, *i.e.* the shift of characteristic inter-layer diffraction to higher angles, with the increasing duration of acidic treatment is caused by the consecutive breaking of inter-layer Ge–O(T) bonds; (ii) the stability of the inter-layer diffraction line position after a certain time of hydrolysis indicates that the full destruction of labile (*i.e.* Ge–O(T)) inter-layer bonds has been already achieved; and (iii) the decreasing acid concentration and temperature of the treatment cause the decrease in inter-layer distances (Fig. 18).

High efficiency of low-concentrated acid solutions ($\leq$0.01 M) and low treatment temperature (25 °C) in hydrolysis of germanosilicates **ITH** and **ITR** are consistent with the increasing rate of

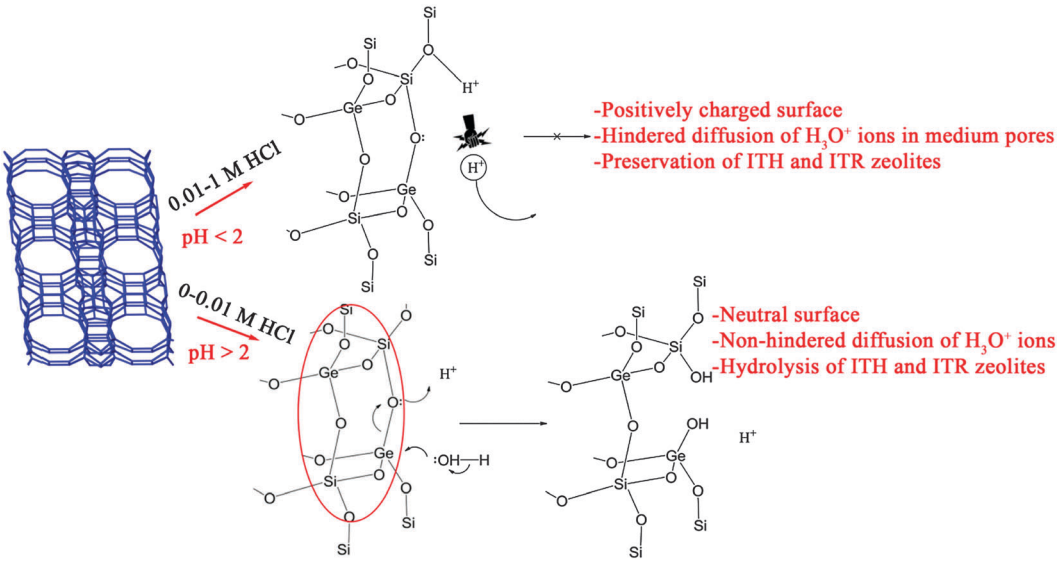

Scheme 2 The influence of pH on the hydrolysis of **ITH** and **ITR** zeolites in acidic media.

competing zeolite reconstruction under harsher treatment conditions ($T > 95$ °C, [HCl] = 3–12 M) as shown for **UTL** zeolites (for more details see Chapter 3).[91] At the same time, diffusion of ions, influenced, in particular, by the acidity of the reaction medium, may play a decisive role in the hydrolysis of medium-pore germanosilicates (*e.g.* **ITH** and **ITR**). From this point of view, the increasing concentration of HCl (in the range pH = 0–2) results in (1) the increase in the positive charge of the zeolite surface; (2) the hindrance of the access of hydroxonium ions to the inter-layer space; (3) and the inhibition of zeolite hydrolysis (Scheme 2).[177]

The behaviour of extra-large pore germanosilicate **UTL** zeolites under hydrolysis conditions can be compared with that of other germanosilicates. The decrease in the *d*-spacing after hydrolysis of **UTL** zeolites to IPC-1P precursors (Δd_{002} 2.75 Å[62]) is close to that for hydrolysed germanosilicates of other topologies (2.62, 1.70, and 2.6 Å for **ITH**, **ITR**, and **IWW** zeolites, respectively).[177] The role of treatment variables (*i.e.* pH, the temperature and duration of the treatment) lies in controlling the rates of two competing processes, *i.e.* de-intercalation (prevailing in low acidic medium at low temperatures) and rearrangement (contributed at elevated temperatures in highly acidic medium). The range of Si/Ge ratios in the parent germanosilicate necessary for full disassembly of silica layers is determined by the topology of the particular zeolite and may require special synthesis conditions to be achieved. In general, it is broader for **UTL** in comparison to **ITH**, **IWR**, **IWW** and especially **ITR** zeolites (Table 4). However, having at least 4 Ge atoms per each D4R and plus their location at appropriate positions (Fig. 14a and b) is a good starting point to successfully disassemble the respective germanosilicates into a lamellar material.[83,203]

Thus, the following factors controlling the disassembly degree of studied germanosilicates can be highlighted:

(1) Size of the pore system. The disassembly of germanosilicate zeolites is a continuous process developing with time. The length of the optimal hydrolysis is likely determined by diffusion of ions into and out of the pore system of germanosilicate zeolites. The rate of acidic hydrolysis increases with the increasing pore size of germanosilicates being higher for extra-large pore **UTL** and large-pore **IWW** zeolites in comparison with medium pore **ITH** and **ITR** zeolites.

(2) Chemical composition and Ge distribution. The Si/Ge ratio in the parent zeolite impacting the number of labile Ge–O(T) inter-layer bonds strongly influences its hydrolytic stability, which decreases with increasing Ge content. Appropriate chemical composition (Si/Ge < 6 for **ITH**, **IWW** and **IWR**, Si/Ge < 3.7 for **ITR** corresponding to $\geq 50\%$ Ge in D4R units) has to match with the proper distribution of Ge atoms in D4Rs to make germanosilicates prospective objects of the selective disassembly process. For zeolites having $\geq 50\%$ of Ge atoms in D4R units, full transformation into a layered material was found. Lowering of the Ge concentration resulted in only a partial separation of crystalline layers or only extraction of Ge atoms while preserving the original framework of germanosilicates. Despite the fact that boron atoms are essential for the formation of **IWR** zeolites as stabilizing elements, with respect to selective hydrolysis of Ge-D4Rs, B–O(T) intra-layer sites actually decrease the stability of the **IWR**-layers. It limits the applicability of borogermanosilicate zeolites as precursors for two-dimensional zeolites.

(3) Acid concentration and temperature. As for the mechanism of **UTL** hydrolysis,[91] for **ITH** and **ITR** it is a complex multistep process including not only hydrolysis but also the possibility of competing rearrangement to rebuild inter-layer connections. The low-concentration acid solutions (<0.01 M) and low treatment temperature (25 °C) do not promote any rearrangement processes that lead to reconnection of the layers and are therefore more efficient for hydrolysis of germanosilicate zeolites under study. One should think of the process to suppress the rebuilding of the inter-layer connection, which might allow a general process for preventing layer reconnection.

12. Isomorphous substitution to prepare active materials

Of course the great interest in zeolites stems from their utility in many different industries. The activity required for applications such as ion exchange and catalysis comes from the substitution of silicon for other, often aliovalent, elements. The most common substituent element is aluminium, whose trivalent nature imparts an overall negative charge on the zeolite framework and necessitates charge-balancing species in the pores of the zeolite to maintain electrical neutrality. Other substituents such as titanium impart other functionalities (for example redox properties).

The ADOR strategy not only allows the design of new structures but there is also the possibility to incorporate substituents to modify the acidity and consequently catalytic properties of respective germanosilicates. In particular, isomorphous incorporation of trivalent elements (B, Al, Ga, Fe) is a common tool to tailor the acidity of zeolites and can be performed in either of the assembly or organisation/reassembly steps of the ADOR process. For example one can prepare Al/Ge-**UTL** during the assembly process – this is the standard method by which **UTL** catalysts are prepared.[76] Given the overwhelming preference of Ge for the D4R units between the layers, this necessarily means that the aluminium is preferentially sited within the layers. Combining this with the fact that the aluminium is much less hydrolytically sensitive than germanium means that the aluminium may be retained during the subsequent disassembly, organisation and reassembly steps, yielding an Al-substituted final material. This strategy was used to prepare an Al-substituted IPC-2 material, which was then tested for catalytic activity in the alkylation of toluene with isopropyl alcohol (Fig. 19). The activity of Al-IPC-2 was similar to **MFI**, and lower than both zeolite **BEA**, which has a highly accessible three dimensional 12-12-12-ring system, and **UTL** (14-12-ring). However, the selectivity to all cymenes was higher than **MFI** and similar to **BEA** and **UTL**, although selectivity to *p*-cymenes was similar to **MFI**. The activity of Al-IPC-4 was much lower, consistent with the smaller channels in this structure (10-8-ring). Nevertheless, using Al-**UTL** for the synthesis of catalytically active IPC zeolites is only one of the approaches, which may be applied. Another one considers the incorporation of aluminium during the hydrolysis as the presence of aluminium can lead to healing of some structural defects, which may be generated during the acidic treatment.

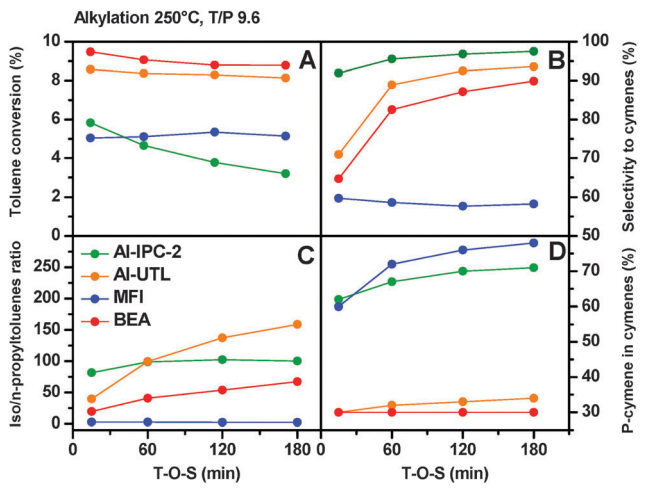

Fig. 19 Time-on-stream dependence of toluene conversion (A), selectivity to cymenes (B), iso-/*n*-propyltoluene ratio (C) and *p*-cymene selectivity (D) in toluene alkylation with isopropyl alcohol at 250 °C for four different zeolites; Al-IPC-2, Al-**UTL**, **MFI** and **BEA**.

An interesting feature of the ADOR process, which has not been fully explored yet, is the possibility of controlling the location of the aluminium sites with much more precision than is currently the case in the organisation step. When the partial removal of Ge from the T sites in D4Rs is performed, aluminium can be incorporated precisely into these positions. Fig. 3 shows the use of $(CH_3)_2Si(OCH_2CH_3)_2$ as an organising agent, which selectively puts silicon into the interlayer space leading to IPC-2 as the final material on reassembly. However, replacing up to half the species with Al-bearing organising agents should lead to a material with Al only in the interlayer sites. This is complementary to the materials discussed above, where aluminium sites are only in the layers. Such synthesis has not yet been completed but offers an interesting new approach to acid site control in zeolites.

13. Perspectives for the ADOR process

The ADOR process described in this review is essentially a new method for manipulating zeolites, which has the potential to revolutionise the way we think about the synthesis of zeolites, and possibly other types of materials as well. The process relies on the recognition that a chemical 'weakness' in a prepared solid can be exploited to manipulate the materials into new structures. The potential importance of the ADOR mechanism lies in three areas

(i) The ability to make new materials such as IPC-2, IPC-4, IPC-6 and IPC-7 zeolites.

(ii) The introduction of new concepts that impart novel functionality or new levels of control over materials, such as the continuous control over zeolite porosity described in Section 7 and Fig. 8.

(iii) The ability to challenge traditional hydrothermal synthesis methods as a way of producing important zeolite materials, either by producing a significant number of new materials or by producing materials that are not possible using the traditional methods.

Points (i) and (ii) have essentially been proved by the work that has been described in the body of this review. Point (iii) on the other hand is the major goal of the ongoing research on the ADOR method at the moment, but is yet to be proved. This can be translated into the following items

(1) Utilization of the ADOR protocol for other germanosilicates in addition to **UTL**. This partly has been already achieved and it is discussed *vide supra*.

(2) Investigation of the role of other heteroatoms introducing local instability, like B or Ga and their utilization for similar transformations.

(3) A challenging approach to find a similar protocol for zeolites without liable heteroatoms, maybe based on different bond densities throughout the framework.

One of the enduring mysteries of zeolite synthesis is why there are so few frameworks known. There are just over 200 different zeolite topologies currently known, and about 40–50 of these can be made as pure or very high as a silica phase. This is in contrast with the computational work that predicts that there are millions of different ways to connect silica tetrahedral into zeolite-like materials. Morris and Čejka in a Nature Chemistry[129] perspective argue that this mismatch between the theoretically possible and experimentally reached conclusions is due to an intrinsic limitation of the traditional synthetic methodology and that new methods of synthesis, such as the ADOR process, are required if we intend to fully exploit the potential of zeolites of all types. Already, the ADOR process has led to several new silica zeolites, and if the predictions made in the literature for the number of zeolites that could be prepared using the ADOR process are borne out, it could rival or even eclipse the number of similar zeolites prepared using traditional methods over the next decade or so. This is where the real importance of the ADOR process will be found.

Acknowledgements

This work was supported by the Czech Science Foundation Grant No. P106/12/G015 (Centre of Excellence) and Grant No. 14-30898P (MS only). W.J.R acknowledges partial financial support provided by the National Science Centre Poland with a grant approved under No. DEC-2011/03/B/ST5/01551. R.E.M. thanks the Royal Society for provision of an industry fellowship and the E.P.S.R.C. for funding (EP/K025112/1 and EP/L014475/1).

References

1 C. Martinez and A. Corma, *Coord. Chem. Rev.*, 2011, **255**, 1558–1580.
2 C. Martínez and A. Corma, in *Comprehensive Inorganic Chemistry II*, ed. J. R. Poeppelmeier, Elsevier, Amsterdam, 2nd edn, 2013, pp. 103–131.
3 D. W. Breck, *J. Chem. Educ.*, 1964, **41**, 678–689.
4 D. W. Breck, *Zeolite molecular sieves: structure, chemistry, and use*, Wiley, New York, 1973.
5 J. Gascon, F. Kapteijn, B. Zornoza, V. Sebastian, C. Casado and J. Coronas, *Chem. Mater.*, 2012, **24**, 2829–2844.
6 N. Kosinov, C. Auffret, V. G. P. Sripathi, C. Gucuyener, J. Gascon, F. Kapteijn and E. J. M. Hensen, *Microporous Mesoporous Mater.*, 2014, **197**, 268–277.
7 O. Cheung and N. Hedin, *RSC Adv.*, 2014, **4**, 14480–14494.
8 M. Mofarahi and F. Gholipour, *Microporous Mesoporous Mater.*, 2014, **200**, 1–10.
9 M. Anderson, H. Wang and Y. S. Lin, *Rev. Chem. Eng.*, 2012, **28**, 101–121.
10 M. Moliner, *Dalton Trans.*, 2014, **43**, 4197–4208.
11 A. Primo and H. Garcia, *Chem. Soc. Rev.*, 2014, **43**, 7548–7561.
12 T. J. Schwartz, B. J. O'Neill, B. H. Shanks and J. A. Dumesic, *ACS Catal.*, 2014, **4**, 2060–2069.
13 K. Li, J. Valla and J. Garcia-Martinez, *ChemCatChem*, 2014, **6**, 46–66.
14 I. Fechete, Y. Wang and J. C. Védrine, *Catal. Today*, 2012, **189**, 2–27.
15 R. Moos, *Sensors*, 2010, **10**, 6773–6787.
16 M. P. Pina, R. Mallada, M. Arruebo, M. Urbiztondo, N. Navascues, O. de la Iglesia and J. Santamaria, *Microporous Mesoporous Mater.*, 2011, **144**, 19–27.
17 A. Babaei, B. Khalilzadeh and M. Afrasiabi, *J. Appl. Electrochem.*, 2010, **40**, 1537–1543.
18 J. V. Smith, *Chem. Rev.*, 1988, **88**, 149–182.
19 C. Baerlocher, L. B. McCusker and D. H. Olson, *Atlas of Zeolite Framework Types*, Elsevier, Amsterdam, 2007.
20 C. S. Cundy and P. A. Cox, *Chem. Rev.*, 2003, **103**, 663–701.
21 M. E. Davis and R. F. Lobo, *Chem. Mater.*, 1992, **4**, 756–768.
22 C. S. Cundy and P. A. Cox, *Microporous Mesoporous Mater.*, 2005, **82**, 1–78.
23 J. E. Schmidt, M. W. Deem and M. E. Davis, *Angew. Chem., Int. Ed.*, 2014, **53**, 8372–8374.
24 L. Gomez-Hortigueela, F. Lopez-Arbeloa, F. Cora and J. Perez-Pariente, *J. Am. Chem. Soc.*, 2008, **130**, 13274–13284.
25 A. Jackowski, S. I. Zones, S.-J. Hwang and A. W. Burton, *J. Am. Chem. Soc.*, 2009, **131**, 1092–1100.
26 R. M. Shayib, N. C. George, R. Seshadri, A. W. Burton, S. I. Zones and B. F. Chmelka, *J. Am. Chem. Soc.*, 2011, **133**, 18728–18741.
27 M. Moliner, F. Rey and A. Corma, *Angew. Chem., Int. Ed.*, 2013, **52**, 13880–13889.
28 A. B. Pinar, L. Gomez-Hortigueela, L. B. McCusker and J. Perez-Pariente, *Chem. Mater.*, 2013, **25**, 3654–3661.
29 A. B. Pinar, C. Marquez-Alvarez, M. Grande-Casas and J. Perez-Pariente, *J. Catal.*, 2009, **263**, 258–265.
30 A. W. Burton and S. I. Zones, *Stud. Surf. Sci. Catal.*, 2007, **168**, 137–179.
31 W. J. Roth, C. T. Kresge, J. C. Vartuli, M. E. Leonowicz, A. S. Fung and S. B. McCullen, *Stud. Surf. Sci. Catal.*, 1995, **94**, 301–308.
32 S. L. Lawton, A. S. Fung, G. J. Kennedy, L. B. Alemany, C. D. Chang, G. H. Hatzikos, D. N. Lissy, M. K. Rubin, H.-K. C. Timken, S. Steuernagel and D. E. Woessner, *J. Phys. Chem.*, 1996, **100**, 3788–3798.
33 R. Millini, G. Perego, W. O. Parker Jr, G. Bellussi and L. Carluccio, *Microporous Mater.*, 1995, **4**, 221–230.
34 W. J. Roth and J. Čejka, *Catal. Sci. Technol.*, 2011, **1**, 43–53.
35 W. J. Roth, P. Nachtigall, R. E. Morris and J. Čejka, *Chem. Rev.*, 2014, **114**, 4807–4837.
36 F. S. O. Ramos, M. K. D. Pietre and H. O. Pastore, *RSC Adv.*, 2013, **3**, 2084–2111.
37 U. Diaz and A. Corma, *Dalton Trans.*, 2014, **43**, 10292–10316.

38 T. Selvam, A. Inayat and W. Schwieger, *Dalton Trans.*, 2014, **43**, 10365–10387.
39 B. Marler and H. Gies, *Eur. J. Mineral.*, 2012, **24**, 405–428.
40 W. J. Roth, *Stud. Surf. Sci. Catal.*, 2005, **158A**, 19–26.
41 W. J. Roth, D. L. Dorset and G. J. Kennedy, *Microporous Mesoporous Mater.*, 2011, **142**, 168–177.
42 M. Choi, K. Na, J. Kim, Y. Sakamoto, O. Terasaki and R. Ryoo, *Nature*, 2009, **461**, 246–249.
43 J.-C. Kim, R. Ryoo, M. V. Opanasenko, M. V. Shamzhy and J. Čejka, *ACS Catal.*, 2015, **5**, 2596–2604.
44 C. Jo, K. Cho, J. Kim and R. Ryoo, *Chem. Commun.*, 2014, **50**, 4175–4177.
45 X. Zhang, D. Liu, D. Xu, S. Asahina, K. A. Cychosz, K. V. Agrawal, Y. Al Wahedi, A. Bhan, S. Al Hashimi, O. Terasaki, M. Thommes and M. Tsapatsis, *Science*, 2012, **336**, 1684–1687.
46 P. S. Wheatley and R. E. Morris, *J. Mater. Chem.*, 2006, **16**, 1035–1037.
47 Y. Asakura, R. Takayama, T. Shibue and K. Kuroda, *Chem. – Eur. J.*, 2014, **20**, 1893–1900.
48 A. Rojas and M. A. Camblor, *Chem. Mater.*, 2014, **26**, 1161–1169.
49 W. J. Roth and D. L. Dorset, *Microporous Mesoporous Mater.*, 2011, **142**, 32–36.
50 Y. X. Wang, H. Gies and J. H. Lin, *Chem. Mater.*, 2007, **19**, 4181–4188.
51 B. Marler, N. Stroter and H. Gies, *Microporous Mesoporous Mater.*, 2005, **83**, 201–211.
52 T. Moteki, W. Chaikittisilp, A. Shimojima and T. Okubo, *J. Am. Chem. Soc.*, 2008, **130**, 15780–15781.
53 W. J. Roth and D. L. Dorset, *Struct. Chem.*, 2010, **21**, 385–390.
54 S. Zanardi, A. Alberti, G. Cruciani, A. Corma, V. Fornes and M. Brunelli, *Angew. Chem., Int. Ed.*, 2004, **43**, 4933–4937.
55 T. Ikeda, Y. Akiyama, Y. Oumi, A. Kawai and F. Mizukami, *Angew. Chem., Int. Ed.*, 2004, **43**, 4892–4896.
56 B. Yang, J.-g. Jiang, H. Xu, Y. Liu, H. Peng and P. Wu, *Appl. Catal., A*, 2013, **455**, 107–113.
57 W. J. Roth, *Stud. Surf. Sci. Catal.*, 2007, **168**, 221–239.
58 W. J. Roth and J. C. Vartuli, *Stud. Surf. Sci. Catal.*, 2002, **141**, 273–279.
59 W. J. Roth, B. Gil and B. Marszalek, *Catal. Today*, 2014, **227**, 9–14.
60 M. E. Leonowicz, J. A. Lawton, S. L. Lawton and M. K. Rubin, *Science*, 1994, **264**, 1910–1913.
61 W. Park, D. Yu, K. Na, K. E. Jelfs, B. Slater, Y. Sakamoto and R. Ryoo, *Chem. Mater.*, 2011, **23**, 5131–5137.
62 W. J. Roth, O. V. Shvets, M. Shamzhy, P. Chlubná, M. Kubů, P. Nachtigall and J. Čejka, *J. Am. Chem. Soc.*, 2011, **133**, 6130–6133.
63 W. J. Roth, P. Nachtigall, R. E. Morris, P. S. Wheatley, V. R. Seymour, S. E. Ashbrook, P. Chlubná, L. Grajciar, M. Položij, A. Zukal, O. Shvets and J. Čejka, *Nat. Chem.*, 2013, **5**, 628–633.
64 J. Jung, C. Jo, K. Cho and R. Ryoo, *J. Mater. Chem.*, 2012, **22**, 4637–4640.
65 W. Kim, J.-C. Kim, J. Kim, Y. Seo and R. Ryoo, *ACS Catal.*, 2013, **3**, 192–195.
66 J.-C. Kim, K. Cho, S. Lee and R. Ryoo, *Catal. Today*, 2015, **243**, 103–108.
67 Y. Seo, K. Cho, Y. Jung and R. Ryoo, *ACS Catal.*, 2013, **3**, 713–720.
68 M. V. Opanasenko, M. V. Shamzhy, C. Jo, R. Ryoo and J. Čejka, *ChemCatChem*, 2014, **6**, 1919–1927.
69 O. V. Shvets, P. Nachtigall, W. J. Roth and J. Čejka, *Microporous Mesoporous Mater.*, 2013, **182**, 229–238.
70 C. Baerlocher and L. B. McCusker, Database of Zeolite Structures, http://www.iza-structure.org/databases/.
71 A. Corma, M. J. Diaz-Cabanas, F. Rey, S. Nicolopoulus and K. Boulahya, *Chem. Commun.*, 2004, 1356–1357.
72 J. L. Paillaud, B. Harbuzaru, J. Patarin and N. Bats, *Science*, 2004, **304**, 990–992.
73 O. V. Shvets, N. Kasian, A. Zukal, J. Pinkas and J. Čejka, *Chem. Mater.*, 2010, **22**, 3482–3495.
74 O. V. Shvets, M. V. Shamzhy, P. S. Yaremov, Z. Musilová, D. Procházková and J. Čejka, *Chem. Mater.*, 2011, **23**, 2573–2585.
75 O. V. Shvets, A. Zukal, N. Kasian, N. Žilková and J. Čejka, *Chem. – Eur. J.*, 2008, **14**, 10134–10140.
76 M. V. Shamzhy, O. V. Shvets, M. V. Opanasenko, P. S. Yaremov, L. G. Sarkisyan, P. Chlubná, A. Zukal, V. R. Marthala, M. Hartmann and J. Čejka, *J. Mater. Chem.*, 2012, **22**, 15793–15803.
77 T. Blasco, A. Corma, M. J. Diaz-Cabanas, F. Rey, J. A. Vidal-Moya and C. M. Zicovich-Wilson, *J. Phys. Chem. B*, 2002, **106**, 2634–2642.
78 A. Corma, M. J. Diaz-Cabanas, J. Martinez-Triguero, F. Rey and J. Rius, *Nature*, 2002, **418**, 514–517.
79 A. Pulido, G. Sastre and A. Corma, *ChemPhysChem*, 2006, **7**, 1092–1099.
80 G. Sastre, A. Pulido and A. Corma, *Microporous Mesoporous Mater.*, 2005, **82**, 159–163.
81 A. Corma, F. Rey, S. Valencia, J. L. Jorda and J. Rius, *Nat. Mater.*, 2003, **2**, 493–497.
82 J. A. Vidal-Moya, T. Blasco, F. Rey, A. Corma and M. Puche, *Chem. Mater.*, 2003, **15**, 3961–3963.
83 N. Kasian, A. Tuel, E. Verheyen, C. E. A. Kirschhock, F. Taulelle and J. A. Martens, *Chem. Mater.*, 2014, **26**, 5556–5565.
84 Q. Li, A. Navrotsky, F. Rey and A. Corma, *Microporous Mesoporous Mater.*, 2003, **59**, 177–183.
85 Q. Li, A. Navrotsky, F. Rey and A. Corma, *Microporous Mesoporous Mater.*, 2004, **74**, 87–92.
86 N. Žilková, M. Shamzhy, O. Shvets and J. Čejka, *Catal. Today*, 2013, **204**, 22–29.
87 M. V. Shamzhy, O. V. Shvets, M. V. Opanasenko, L. Kurfiřtová, D. Kubička and J. Čejka, *ChemCatChem*, 2013, **5**, 1891–1898.
88 H. Xu, J. Jiang, B. Yang, H. Wu and P. Wu, *Catal. Commun.*, 2014, **55**, 83–86.
89 N. Kasian, G. Vanbutsele, K. Houthoofd, T. I. Koranyi, J. A. Martens and C. E. A. Kirschhock, *Catal. Sci. Technol.*, 2011, **1**, 246–254.

90 A. Corma, U. Diaz, M. E. Domine and V. Fornés, *Angew. Chem., Int. Ed.*, 2000, **39**, 1499–1501.
91 P. S. Wheatley, P. Chlubná-Eliášová, H. Greer, W. Zhou, V. R. Seymour, D. M. Dawson, S. E. Ashbrook, A. B. Pinar, L. B. McCusker, M. Opanasenko, J. Čejka and R. E. Morris, *Angew. Chem., Int. Ed.*, 2014, **126**, 13426–13430.
92 P. Chlubná, W. J. Roth, H. F. Greer, W. Z. Zhou, O. Shvets, A. Zukal, J. Čejka and R. E. Morris, *Chem. Mater.*, 2013, **25**, 542–547.
93 R. L. Smith, P. Eliášová, M. Mazur, M. P. Attfield, J. Čejka and M. W. Anderson, *Chem. – Eur. J.*, 2014, **20**, 10446–10450.
94 W. J. Roth and C. T. Kresge, *Microporous Mesoporous Mater.*, 2011, **144**, 158–161.
95 J. Hermann, M. Trachta, P. Nachtigall and O. Bludský, *Catal. Today*, 2014, **227**, 2–8.
96 L. Grajciar, O. Bludský, W. J. Roth and P. Nachtigall, *Catal. Today*, 2013, **204**, 15–21.
97 M. Mazur, P. Chlubná-Eliášová, W. J. Roth and J. Čejka, *Catal. Today*, 2014, **227**, 37–44.
98 J. Shin, N. H. Ahn, M. A. Camblor, S. J. Cho and S. B. Hong, *Angew. Chem., Int. Ed.*, 2014, **53**, 8949–8952.
99 T. Ikeda, S. Inagaki, T.-a. Hanaoka and Y. Kubota, *J. Phys. Chem. C*, 2010, **114**, 19641–19648.
100 R. K. Iller, *The Chemistry of Silica: Solubility, Polymerization, Colloid and Surface Properties, and Biochemistry*, Wiley-Blackwell, Oxford, 1979.
101 S. J. Andrews, M. Z. Papiz, R. McMeeking, A. J. Blake, B. M. Lowe, K. R. Franklin, J. R. Helliwell and M. M. Harding, *Acta Crystallogr., Sect. B: Struct. Sci.*, 1988, **44**, 73–77.
102 L. Schreyeck, P. Caullet, J. C. Mougenel, J. L. Guth and B. Marler, *Microporous Mater.*, 1996, **6**, 259–271.
103 B. Marler, Y. Wang, J. Song and H. Gies, *Dalton Trans.*, 2014, **43**, 10396–10416.
104 P. Wu, J. F. Ruan, L. L. Wang, L. L. Wu, Y. Wang, Y. M. Liu, W. B. Fan, M. Y. He, O. Terasaki and T. Tatsumi, *J. Am. Chem. Soc.*, 2008, **130**, 8178–8187.
105 W. B. Fan, P. Wu, S. Namba and T. Tatsumi, *Angew. Chem., Int. Ed.*, 2004, **43**, 236–240.
106 L. B. McCusker and C. Baerlocher, *Stud. Surf. Sci. Catal.*, 2005, **157**, 41–64.
107 M. Mazur, M. Kubů, P. S. Wheatley and P. Eliášová, *Catal. Today*, 2015, **243**, 23–31.
108 M. Trachta, O. Bludský, J. Čejka, R. E. Morris and P. Nachtigall, *ChemPhysChem*, 2014, **15**, 2972–2976.
109 H. V. Thang, M. Rubeš, O. Bludský and P. Nachtigall, *J. Phys. Chem. A*, 2014, **118**, 7526–7534.
110 M. Trachta, P. Nachtigall and O. Bludský, *Catal. Today*, 2015, **243**, 32–38.
111 A. Rimola, D. Costa, M. Sodupe, J.-F. Lambert and P. Ugliengo, *Chem. Rev.*, 2013, **113**, 4216–4313.
112 Z. Zhao, W. Zhang, P. Ren, X. Han, U. Müller, B. Yilmaz, M. Feyen, H. Gies, F.-S. Xiao, D. De Vos, T. Tatsumi and X. Bao, *Chem. Mater.*, 2013, **25**, 840–847.
113 O. Bludský, M. Rubeš, P. Soldán and P. Nachtigall, *J. Chem. Phys.*, 2008, **128**, 114102.
114 J. Hermann and O. Bludský, *J. Chem. Phys.*, 2013, **139**, 034115.
115 D. Nachtigallová, P. Nachtigall and O. Bludský, *Phys. Chem. Chem. Phys.*, 2004, **6**, 5580–5587.
116 R. Pophale, P. A. Cheeseman and M. W. Deem, *Phys. Chem. Chem. Phys.*, 2011, **13**, 12407–12412.
117 D. Majda, F. A. A. Paz, O. D. Friedrichs, M. D. Foster, A. Simperler, R. G. Bell and J. Klinowski, *J. Phys. Chem. C*, 2008, **112**, 1040–1047.
118 Y. Li, J. Yu and R. Xu, *Angew. Chem., Int. Ed.*, 2013, **52**, 1673–1677.
119 E. Verheyen, L. Joos, K. Van Havenbergh, E. Breynaert, N. Kasian, E. Gobechiya, K. Houthoofd, C. Martineau, M. Hinterstein, F. Taulelle, V. Van Speybroeck, M. Waroquier, S. Bals, G. Van Tendeloo, C. E. A. Kirschhock and J. A. Martens, *Nat. Mater.*, 2012, **11**, 1059–1064.
120 M. S. Whittingham and A. J. Jacobson, *Intercalation Chemistry*, Academic Press, New York, 1982.
121 S. M. Auerbach, K. A. Carrado and P. K. Dutta, *Handbook of Layered Materials*, Marcel Dekker, New York, 2004.
122 A. Lerf, *Dalton Trans.*, 2014, **43**, 10276–10291.
123 K. Ohtsuka, *Chem. Mater.*, 1997, **9**, 2039–2050.
124 N. Takabashi, H. Hata and K. Kuroda, *Chem. Mater.*, 2011, **23**, 266–273.
125 K. Fukuda, J. Sato, T. Saida, W. Sugimoto, Y. Ebina, T. Shibata, M. Osada and T. Sasaki, *Inorg. Chem.*, 2013, **52**, 2280–2282.
126 L. Pauling, *Zeitschrift fuer Kristallographie and Mineralogie*, 1930, **74**, 213.
127 T. R. Macedo and C. Airoldi, *Microporous Mesoporous Mater.*, 2010, **128**, 158–164.
128 M. Shamzhy, M. Mazur, M. Opanasenko, W. J. Roth and J. Čejka, *Dalton Trans.*, 2014, **43**, 10548–10557.
129 R. E. Morris and J. Cejka, *Nat. Chem.*, 2015, **7**, 381–388.
130 M. E. Landis, B. A. Aufdembrink, P. Chu, I. D. Johnson, G. W. Kirker and M. K. Rubin, *J. Am. Chem. Soc.*, 1991, **113**, 3189–3190.
131 A. Zukal and M. Kubů, *Dalton Trans.*, 2014, **43**, 10558–10565.
132 Y. J. He, G. S. Nivarthy, F. Eder, K. Seshan and J. A. Lercher, *Microporous Mesoporous Mater.*, 1998, **25**, 207–224.
133 A. Corma, V. Fornés, J. Martínez-Triguero and S. B. Pergher, *J. Catal.*, 1999, **186**, 57–63.
134 A. Corma, V. Fornés, J. M. Guil, S. Pergher, T. L. M. Maesen and J. G. Buglass, *Microporous Mesoporous Mater.*, 2000, **38**, 301–309.
135 E. Dumitriu, I. Fechete, P. Caullet, H. Kessler, V. Hulea, C. Chelaru, I. Hulea and X. Bourdon, *Stud. Surf. Sci. Catal.*, 2002, **142**, 951–958.
136 E. Dumitriu, F. Secundo, J. Patarin and I. Fechete, *J. Mol. Catal. B: Enzym.*, 2003, **22**, 119–133.
137 J.-O. Barth, A. Jentys, J. Kornatowski and J. A. Lercher, *Chem. Mater.*, 2004, **16**, 724–730.
138 J.-O. Barth, A. Jentys, E. F. Iliopoulou, I. A. Vasalos and J. A. Lercher, *J. Catal.*, 2004, **227**, 117–129.
139 S. Laforge, P. Ayrault, D. Martin and M. Guisnet, *Appl. Catal., A*, 2005, **279**, 79–88.

140 B. Gil, W. Makowski, B. Marszalek, W. J. Roth, M. Kubů, J. Čejka and Z. Olejniczak, *Dalton Trans.*, 2014, **43**, 10501–10511.
141 J.-O. Barth, J. Kornatowski and J. A. Lercher, *J. Mater. Chem.*, 2002, **12**, 369–373.
142 A. Corma, U. Díaz, T. García, G. Sastre and A. Velty, *J. Am. Chem. Soc.*, 2010, **132**, 15011–15021.
143 M. Opanasenko, W. O. N. Parker, M. Shamzhy, E. Montanari, M. Bellettato, M. Mazur, R. Millini and J. Čejka, *J. Am. Chem. Soc.*, 2014, **136**, 2511–2519.
144 T. Blasco, *J. Phys. Chem. B*, 2002, **106**, 2634–2642.
145 H. Li and O. M. Yaghi, *J. Am. Chem. Soc.*, 1998, **120**, 10569–10570.
146 Y. Mathieu, J.-L. Paillaud, P. Caullet and N. Bats, *Microporous Mesoporous Mater.*, 2004, **75**, 13–22.
147 D. S. Wragg, R. E. Morris and A. W. Burton, *Chem. Mater.*, 2008, **20**, 1561–1570.
148 M. A. Zwijnenburg, S. T. Bromley, J. C. Jansen and T. Maschmeyer, *Microporous Mesoporous Mater.*, 2004, **73**, 171–174.
149 T. Conradsson, M. S. Dadachov and X. D. Zou, *Microporous Mesoporous Mater.*, 2000, **41**, 183–191.
150 J. X. Jiang, J. L. Jorda, M. J. Diaz-Cabanas, J. H. Yu and A. Corma, *Angew. Chem., Int. Ed.*, 2010, **49**, 4986–4988.
151 J. X. Jiang, J. H. Yu and A. Corma, *Angew. Chem., Int. Ed.*, 2010, **49**, 3120–3145.
152 M. Moliner, T. Willhammar, W. Wan, J. González, F. Rey, J. L. Jorda, X. Zou and A. Corma, *J. Am. Chem. Soc.*, 2012, **134**, 6473–6478.
153 A. Corma, M. Puche, F. Rey, G. Sankar and S. J. Teat, *Angew. Chem., Int. Ed.*, 2003, **42**, 1156–1159.
154 A. Corma, M. J. Diaz-Cabanas, J. L. Jorda, F. Rey, G. Sastre and K. G. Strohmaier, *J. Am. Chem. Soc.*, 2008, **130**, 16482–16483.
155 A. Corma, M. J. Diaz-Cabanas, J. L. Jorda, C. Martinez and M. Moliner, *Nature*, 2006, **443**, 842–845.
156 J. Sun, C. Bonneau, A. Cantin, A. Corma, M. J. Diaz-Cabanas, M. Moliner, D. Zhang, M. Li and X. Zou, *Nature*, 2009, **458**, 1154–1157.
157 D. L. Dorset, K. G. Strohmaier, C. E. Kliewer, A. Corma, M. J. Diaz-Cabanas, F. Rey and C. J. Gilmore, *Chem. Mater.*, 2008, **20**, 5325–5331.
158 L. Tang, L. Shi, C. Bonneau, J. Sun, H. Yue, A. Ojuva, B.-L. Lee, M. Kritikos, R. G. Bell, Z. Bacsik, J. Mink and X. Zou, *Nat. Mater.*, 2008, **7**, 381–385.
159 D. J. Earl, A. W. Burton, T. Rea, K. Ong, M. W. Deem, S.-J. Hwang and S. I. Zones, *J. Phys. Chem. C*, 2008, **112**, 9099–9105.
160 Y. Lorgouilloux, M. Dodin, J.-L. Paillaud, P. Caullet, L. Michelin, L. Josien, O. Ersen and N. Bats, *J. Solid State Chem.*, 2009, **182**, 622–629.
161 M. Dodin, J.-L. Paillaud, Y. Lorgouilloux, P. Caullet, E. Elkaïm and N. Bats, *J. Am. Chem. Soc.*, 2010, **132**, 10221–10223.
162 M. Hernández-Rodríguez, J. L. Jordá, F. Rey and A. Corma, *J. Am. Chem. Soc.*, 2012, **134**, 13232–13235.
163 W. Hua, H. Chen, Z.-B. Yu, X. Zou, J. Lin and J. Sun, *Angew. Chem., Int. Ed.*, 2014, **53**, 5868–5871.
164 A. Corma, M. J. Diaz-Cabanas, J. Jiang, M. Afeworki, D. L. Dorset, S. L. Soled and K. G. Strohmaier, *Proc. Natl. Acad. Sci. U. S. A.*, 2010, **107**, 13997–14002.
165 R. Castaneda, A. Corma, V. Fornes, F. Rey and J. Rius, *J. Am. Chem. Soc.*, 2003, **125**, 7820–7821.
166 T. B. Reed and D. W. Breck, *J. Am. Chem. Soc.*, 1956, **78**, 5972–5977.
167 D. L. Dorset, G. J. Kennedy, K. G. Strohmaier, M. J. Diaz-Cabañas, F. Rey and A. Corma, *J. Am. Chem. Soc.*, 2006, **128**, 8862–8867.
168 C. S. Blackwell, R. W. Broach, M. G. Gatter, J. S. Holmgren, D.-Y. Jan, G. J. Lewis, B. J. Mezza, T. M. Mezza, M. A. Miller, J. G. Moscoso, R. L. Patton, L. M. Rohde, M. W. Schoonover, W. Sinkler, B. A. Wilson and S. T. Wilson, *Angew. Chem., Int. Ed.*, 2003, **42**, 1737–1740.
169 R. Simancas, J. L. Jordá, F. Rey, A. Corma, A. Cantín, I. Peral and C. Popescu, *J. Am. Chem. Soc.*, 2014, **136**, 3342–3345.
170 J. L. Jordá, F. Rey, G. Sastre, S. Valencia, M. Palomino, A. Corma, A. Segura, D. Errandonea, R. Lacomba, F. J. Manjón, Ó. Gomis, A. K. Kleppe, A. P. Jephcoat, M. Amboage and J. A. Rodríguez-Velamazán, *Angew. Chem., Int. Ed.*, 2013, **52**, 10458–10462.
171 Y. Lorgouilloux, M. Dodin, E. Mugnaioli, C. Marichal, P. Caullet, N. Bats, U. Kolb and J.-L. Paillaud, *RSC Adv.*, 2014, **4**, 19440–19449.
172 J. Michael Bennett and R. M. Kirchner, *Zeolites*, 1991, **11**, 502–506.
173 J. M. Bennett and B. K. Marcus, *Stud. Surf. Sci. Catal.*, 1988, **37**, 269–279.
174 A. Corma, F. Rey, J. Rius, M. J. Sabater and S. Valencia, *Nature*, 2004, **431**, 287–290.
175 M. W. Simon, S. S. Nam, W. Q. Xu, S. L. Suib, J. C. Edwards and C. L. O'Young, *J. Phys. Chem.*, 1992, **96**, 6381–6388.
176 W. Zhou, S.-Y. Zhang, X.-Y. Hao, H. Guo, C. Zhang, Y.-Q. Zhang and S. Liu, *J. Solid State Chem.*, 2006, **179**, 855–865.
177 M. Shamzhy, M. Opanasenko, Y. Tian, K. Konysheva, O. Shvets, R. E. Morris and J. Čejka, *Chem. Mater.*, 2014, **26**, 5789–5798.
178 D. Goldfarb, M. Bernardo, K. G. Strohmaier, D. E. W. Vaughan and H. Thomann, *J. Am. Chem. Soc.*, 1994, **116**, 6344–6353.
179 B. Gil, B. Marszalek, A. Adamski, Z. Olejniczak, M. Kubů and J. Čejka, *Microporous Mesoporous Mater.*, 2012, **151**, 339–345.
180 M. Moliner, T. Willhammar, W. Wan, J. Gonzalez, F. Rey, J. L. Jorda, X. D. Zou and A. Corma, *J. Am. Chem. Soc.*, 2012, **134**, 6473–6478.
181 A. Corma, M. J. Diaz-Cabanas, J. L. Jorda, C. Martinez and M. Moliner, *Nature*, 2006, **443**, 842–845.
182 J. X. Jiang, J. L. Jorda, J. H. Yu, L. A. Baumes, E. Mugnaioli, M. J. Diaz-Cabanas, U. Kolb and A. Corma, *Science*, 2011, **333**, 1131–1134.

183 M. E. Davis, C. Saldarriaga, C. Montes, J. Garces and C. Crowdert, *Nature*, 1988, **331**, 698–699.
184 J. V. Smith and W. J. Dytrych, *Nature*, 1984, **309**, 607–608.
185 A. Corma, M. T. Navarro, F. Rey, J. Rius and S. Valencia, *Angew. Chem., Int. Ed.*, 2001, **40**, 2277–2280.
186 J. M. Newsam, M. M. J. Treacy, W. T. Koetsier and C. B. D. Gruyter, *Proc. R. Soc. A*, 1988, **420**, 375–405.
187 D. L. Dorset, W. J. Roth, G. J. Kennedy and S. S. Dhingra, *Z. Kristallogr.*, 2008, **223**, 456.
188 M. J. Sanders, M. Leslie and C. R. A. Catlow, *J. Chem. Soc., Chem. Commun.*, 1984, 1271–1273.
189 K. P. Schroder, J. Sauer, M. Leslie, C. R. A. Catlow and J. M. Thomas, *Chem. Phys. Lett.*, 1992, **188**, 320–325.
190 M. D. Foster and M. M. J. Treacy, Database of Hypothetical Zeolite Structures, http://www.hypotheticalzeolites.net.
191 B. B. Schaack, W. Schrader and T. Schueth, *Angew. Chem., Int. Ed.*, 2008, **47**, 9092–9095.
192 R. Castaneda, A. Corma, V. Fornes, J. Martinez-Triguero and S. Valencia, *J. Catal.*, 2006, **238**, 79–87.
193 G. Sastre, A. Pulido, R. Castañeda and A. Corma, *J. Phys. Chem. B*, 2004, **108**, 8830–8835.
194 G. Sastre, A. Pulido and A. Corma, *Microporous Mesoporous Mater.*, 2005, **82**, 159–163.
195 A. Corma, M. J. Diaz-Cabanas, F. Rey, S. Nicolooulas and K. Boulahya, *Chem. Commun.*, 2004, 1356–1357.
196 A. Corma, M. J. Diaz-Cabanas, J. Luis Jorda, C. Martinez and M. Moliner, *Nature*, 2006, **443**, 842–845.
197 J. Jiang, J. L. Jorda, M. J. Diaz-Cabanas, J. Yu and A. Corma, *Angew. Chem., Int. Ed.*, 2010, **49**, 4986–4988.
198 A. Corma, M. J. Diaz-Cabanas, J. L. Jorda, F. Rey, G. Sastre and K. G. Strohmaier, *J. Am. Chem. Soc.*, 2008, **130**, 16482–16483.
199 A. Corma, F. Rey, S. Valencia, J. L. Jorda and J. Rius, *Nat. Mater.*, 2003, **2**, 493–497.
200 J. L. Jorda, A. Cantin, A. Corma, M. J. Diaz-Cabanas, S. Leiva, M. Moliner, F. Rey, M. J. Sabater and S. Valencia, *Z. Kristallogr.*, 2007, 393–398.
201 L. Burel, N. Kasian and A. Tuel, *Angew. Chem., Int. Ed.*, 2014, **53**, 1360–1363.
202 H. Xu, J.-g. Jiang, B. Yang, L. Zhang, M. He and P. Wu, *Angew. Chem., Int. Ed.*, 2014, **53**, 1355–1359.
203 P. Chlubná-Eliášová, Y. Tian, A. B. Pinar, M. Kubů, J. Čejka and R. E. Morris, *Angew. Chem., Int. Ed.*, 2014, **53**, 7048–7052.
204 X. Li and M. W. Deem, *J. Phys. Chem. C*, 2014, **118**, 15835–15839.
205 X. Ren, J. Liu, Y. Li, J. Yu and R. Xu, *J. Porous Mater.*, 2013, **20**, 975–981.
206 C.-Y. Chen and S. I. Zones, *Zeolites and Catalysis*, Wiley-VCH Verlag GmbH & Co. KGaA, 2010, pp. 155–170.

